BOREAS An international journal of Quaternary research

Evidence of multiple thermokarst lake generations from an 11 800-year-old permafrost core on the northern Seward Peninsula, Alaska

JOSEFINE LENZ, SEBASTIAN WETTERICH, BENJAMIN M. JONES, HANNO MEYER, ANATOLY BOBROV AND GUIDO GROSSE

BOREAS

Lenz, J., Wetterich, S., Jones, B. M., Meyer, H., Bobrov, A. & Grosse, G. 2016 (October): Evidence of multiple thermokarst lake generations from an 11 800-year-old permafrost core on the northern Seward Peninsula, Alaska. *Boreas*, Vol. 45, pp. 584–603. 10.1111/bor.12186. ISSN 0300-9483.

Permafrost degradation influences the morphology, biogeochemical cycling and hydrology of Arctic landscapes over a range of time scales. To reconstruct temporal patterns of early to late Holocene permafrost and thermokarst dynamics, site-specific palaeo-records are needed. Here we present a multi-proxy study of a 350-cm-long permafrost core from a drained lake basin on the northern Seward Peninsula, Alaska, revealing Lateglacial to Holocene thermokarst lake dynamics in a central location of Beringia. Use of radiocarbon dating, micropalaeontology (ostracods and testaceans), sedimentology (grain-size analyses, magnetic susceptibility, tephra analyses), geochemistry (total nitrogen and carbon, total organic carbon, $\delta^{13}C_{org}$) and stable water isotopes ($\delta^{18}O$, δD, d excess) of ground ice allowed the reconstruction of several distinct thermokarst lake phases. These include a pre-lacustrine environment at the base of the core characterized by the Devil Mountain Maar tephra (22 800±280 cal. a BP, Unit A), which has vertically subsided in places due to subsequent development of a deep thermokarst lake that initiated around 11 800 cal. a BP (Unit B). At about 9000 cal. a BP this lake transitioned from a stable depositional environment to a very dynamic lake system (Unit C) characterized by fluctuating lake levels, potentially intermediate wetland development, and expansion and erosion of shore deposits. Complete drainage of this lake occurred at 1060 cal. a BP, including post-drainage sediment freezing from the top down to 154 cm and gradual accumulation of terrestrial peat (Unit D), as well as uniform upward talik refreezing. This core-based reconstruction of multiple thermokarst lake generations since 11 800 cal. a BP improves our understanding of the temporal scales of thermokarst lake development from initiation to drainage, demonstrates complex landscape evolution in the ice-rich permafrost regions of Central Beringia during the Lateglacial and Holocene, and enhances our understanding of biogeochemical cycles in thermokarst-affected regions of the Arctic.

Josefine Lenz (Josefine.Lenz@awi.de), Sebastian Wetterich, Hanno Meyer and Guido Grosse, Department of Periglacial Research, Alfred Wegener Institute, Helmholtz Centre for Polar and Marine Research, Telegraphenberg A43, 14473 Potsdam, Germany; Josefine Lenz and Guido Grosse, Institute for Earth and Environmental Sciences, University of Potsdam, Karl-Liebknecht-Str. 24-25, 14476 Potsdam-Golm, Germany; Benjamin M. Jones, U.S. Geological Survey, Alaska Science Center, 4210 University Drive, Anchorage, AK, USA; Anatoly Bobrov, Faculty of Soil Science, Lomonosov Moscow State University, 1-12 Leninskie Gory, Moscow, Russia; *received 22nd December 2015, accepted 14th April 2016.*

Understanding past environmental change is important for assessing the potential impact of future climate variability on permafrost-influenced landscapes in the Arctic. Permafrost plays a key role in the Earth System because it withdraws a large amount of carbon from the carbon cycle by long-term sequestration into perennially frozen soils (Hugelius *et al.* 2014). However, permafrost, and thus the preservation of frozen carbon, is vulnerable to thaw due to increasing air temperatures, creating the potential for extensive permafrost degradation and the formation of thermokarst landforms (Romanovsky *et al.* 2010; Grosse *et al.* 2011).

Thermokarst lakes form in depressions that result from thawing ice-rich permafrost and melting ground ice (van Everdingen 1998). Widespread thermokarst lake initiation appears to have coincided with the onset of the Holocene as a result of warmer and wetter conditions relative to the Pleistocene (Rampton 1988; Walter *et al.* 2007). Since then, the expansion, shrinkage, coalescence and drainage of thermokarst lakes in ice-rich Arctic coastal lowlands has created a complex periglacial landscape of varying-aged lakes and drained lake basins (Hopkins & Kidd 1988; Jones *et al.* 2012). The potentially cyclical nature of thermokarst lakes forming, draining and reforming in arctic coastal lowlands has been a topic of discussion for several decades (Billings & Peterson 1980; Harry & French 1983; Jorgenson & Shur 2007). While thermokarst lake dynamics have been studied in various permafrost regions with satellite imagery and field observations (e.g. in Alaska: Hinkel *et al.* 2007; Jones *et al.* 2011; Jones & Arp 2015; NW Canada: MacDonald *et al.* 2012; Olthof *et al.* 2015; Siberia: Morgenstern *et al.* 2013; Séjourné *et al.* 2015), observations of site-specific thermokarst lake dynamics occurring over long time scales are scarce. A number of lake sediment records have been studied previously to better understand thermokarst processes (Alaska: Jones *et al.* 2012; Gaglioti *et al.* 2014; Lenz *et al.* 2016; Farquharson *et al.* in press; NW Canada: Michel *et al.* 1989; Lenz *et al.* 2013; Siberia: Kaplina & Lozhkin 1980; Biskaborn *et al.* 2013a,b; Schleusner *et al.* 2015) while a few studies have focused on the characteristics, evolution and role of vegetated drained lake basins with respect to carbon storage and biogeochemical cycling in Arctic coastal lowlands (Hinkel *et al.* 2003; Bockheim *et al.* 2004; Zona *et al.* 2010; Jones *et al.* 2012; Fritz *et al.* in press). However, observations of multiple

DOI 10.1111/bor.12186

thermokarst lake generations within a Lateglacial–Holocene palaeoenvironmental record have not been reported so far even though significant effects on e.g. carbon cycling can be expected.

Here we present a multi-proxy record from a permafrost core taken in a drained thermokarst lake basin located on the northern Seward Peninsula (northwest Alaska) to investigate the complex dynamics in spatially overlapping thermokarst lake generations and the vertical chronosequence of thermokarst lake deposits. The northern Seward Peninsula is of particular interest because of its unique location in Central Beringia, the former non-glaciated land bridge between Eurasia and North America, which not only allowed human migration and population of America during the last deglaciation until about 11 000 years ago (Hopkins 1959) but also enabled long-term permafrost development in a continental climate (French & Millar 2014; Vandenberghe *et al.* 2014). In this region, thick syngenetic permafrost of the Late Pleistocene ice-rich yedoma suite has accumulated (Kanevskiy *et al.* 2011), while deglacial to early Holocene warming and sea-level rise shifted the environmental setting from highly continental to more maritime. Thermokarst lakes formed in this region due to thaw of ice-rich yedoma permafrost (Hopkins & Kidd 1988; Lenz *et al.* 2016) and numerous drained basins characterize the modern morphology of the northern Seward Peninsula (Jones *et al.* 2012). Remote sensing studies of spatially overlapping drained lake basins in conjunction with radiocarbon dating of basal ages indicate that such cycling over longer time scales resulted in up to seven overlapping generations of lake basins (Jones *et al.* 2012; Regmi *et al.* 2012). This spatial overlap and the vertical chronosequence of lacustrine and terrestrial phases probably have profound implications for local stratigraphy and biogeochemical cycling in these lakes (Walter Anthony *et al.* 2014). In particular, there is the potential for lacustrine deposits of different lake generations, interspersed by terrestrial deposits, to be preserved on top of each other in lake-basin cores. In this paper, we address the following research questions: (i) how are maturation of permafrost landscapes and thermokarst dynamics reflected in sedimentary, palaeontological and geochemical proxy data?; (ii) what are the implications of lake development on the northern Seward Peninsula for carbon cycling and large-scale environmental change during the Lateglacial and Holocene?

Study area

The study is based on a 350-cm-long sediment core taken in April 2009 from the centre of a drained thermokarst lake basin located on the Cape Espenberg lowlands, northern Seward Peninsula, NW Alaska (latitude 66°33′57″N, longitude 164°28′53″W, Fig. 1). The northern Seward Peninsula is part of the Bering Land Bridge National Park and Preserve and one of the major lake districts in Alaska, where 7.1% of the surface area is covered with extant lakes >1 ha in area (Arp & Jones 2009). More than 75% of the Cape Espenberg lowlands have been reworked by the formation and drainage of thermokarst lakes (Jones *et al.* 2012). Our drained lake basin (informal name: Mama Rhonda) core site (Kit-43) is located 600 m inland from the Chukchi Sea coast and lies 7.4 m above sea level (m a.s.l., Fig. 1). An extant thermokarst lake, Rhonda Lake, whose area is 80 ha and whose average depth is ~1 m, is located to the south and east of the Kit-43 coring location.

Due to a lower sea level during the Last Glacial Maximum (LGM, 26.5–19 ka BP), the continental shelves of the Bering and Chukchi Sea were widely exposed and our study site was located in the centre of a wide Bering Land Bridge (Hopkins 1967; Kaufman & Hopkins 1985). Continental climate allowed continuous permafrost to develop, which today is approximately 100 m thick (Jorgenson *et al.* 2008) with a mean annual ground temperature that ranges from −5 to −2 °C (Smith *et al.* 2010). Besides remnants of Late Pleistocene yedoma uplands, the local morphology is shaped by Holocene periglacial landscape features like thermo-erosional gullies, pingos and polygonal patterned ground, as well as thermokarst lakes and drained thermokarst lake basins (Hopkins 1967; Jones *et al.* 2011; Regmi *et al.* 2012; Wetterich *et al.* 2012). Non-thermokarst lakes of late Quaternary volcanic origin are also present on the northern Seward Peninsula: The Devil Mountain Maar Lakes located about 16 km south of the coring location were created during multiple phreatomagmatic eruptions at 21 500 cal. a BP (Hopkins 1988; Begét *et al.* 1996). The Devil Mountain Maar tephra is distributed over an area of about 2500 km² and buried the excellently preserved LGM Kitluk palaeosol (Höfle *et al.* 2000; Goetcheus & Birks 2001; Kuzmina *et al.* 2008). The two South and North Killeak Maar lakes formed about 42 000 and >125 000 a BP, respectively, whereas Whitefish Maar is assumed to be 100 000–200 000 years old (Hopkins 1988).

Based on observations from Kotzebue (90 km northeast of the study site), the modern climate is classified as subarctic, with a mean January air temperature of −20 °C, a mean July air temperature of +12 °C and a mean annual air temperature of −6 °C. Average annual precipitation is 230 mm a^{-1}, with more than half of the precipitation falling as rain in summer and early autumn (US National Weather Service data, http://www.ncdc.noaa.gov/).

The region is classified as Bering Tundra (Nowacki *et al.* 2002) and modern vegetation is characterized by *Drepanocladus* spp. and *Sphagnum* spp. as well as wet sedge-moss communities (*Carex aquatilis*, *Eriophorum augustifolium*) in waterlogged acidic habitats, tussock

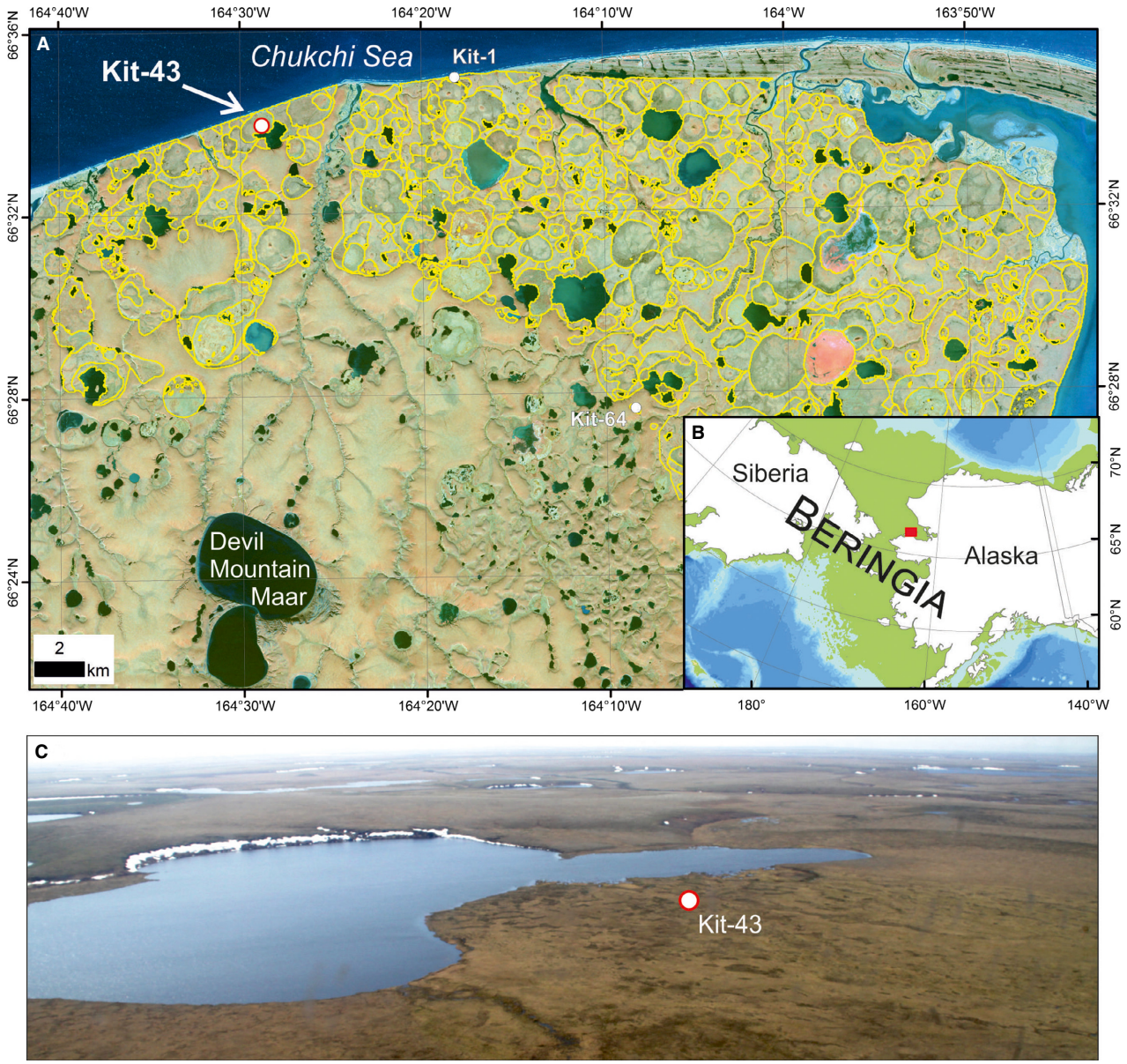

Fig. 1. A. Study area and coring location of Kit-43 as well as location of Kit-1 (Wetterich *et al.* 2012) and Kit-64 (Lenz *et al.* 2016) on the northern Seward Peninsula (©SpotImage Planet Action), which is shaped by numerous drained thermokarst lake basins (yellow circles, see Jones *et al.* 2012) and located in (B) central-eastern Beringia (exposed shelves down to –120 m below modern sea level during the Last Glacial Maximum shown in green colours; Peltier & Fairbanks 2006). C. Aerial photograph of the study site from NE to SW shows modern Lake Rhonda and coring site Kit-43 (white dot). [Colour figure can be viewed at wileyonlinelibrary.com]

sedge (*Eriophorum vaginatum*) and dwarf shrubs (*Ledum palustre*, *Vaccinium vitis-idaea*) on elevated, better-drained sites and erect shrubs (*Andromeda polifolia*, *Betula nana*, *Spiraea beauverdiana*) in drier locations (Wetterich *et al.* 2012).

Material and methods

A 350-cm sediment core (core ID: Kit-43; all depths are given as cm below surface, cm b.s.) was recovered with a SIPRE permafrost corer (Jon Holmgren's Machine Shop, Fairbanks, AK) in April 2009 from the approximate centre of Mama Rhonda basin (Fig. 1). A multi-proxy approach was applied including sedimentological, geochemical and palaeoecological analyses of the sediment as well as isotope geochemical analysis of the intra-sedimentary ice (pore ice and segregated ice).

The frozen core segments were split lengthwise and high-resolution digital photographs were taken with an optical camera system. Mass-specific magnetic susceptibility (MS) was measured at 1-cm intervals at the National Lacustrine Core Facility (LacCore, University of Minnesota) with a multi-sensor core logger (GEOTEK, Bartington-MS2C loop sensor; SI system

is used to express MS values in 10^{-6}). The sediment core halves were then described and stored frozen until subsampling. Subsampling was generally carried out at a 5-cm sampling interval but adapted according to changes of sediment facies.

Pore water was extracted from thawed intra-sedimentary ice with rhizon soil moisture samplers (0.2 μm pore diameter, Eijkelkamp). The hydrogen (δD) and oxygen ($\delta^{18}O$) stable isotope composition of intra-sedimentary ice was analysed with a Picarro L2120i water isotope analyser (as well as with Finnigan MAT Delta-S mass spectrometers for validation, if sample size allowed both measurement techniques). Additional samples taken in the study area in July 2008 from an ice wedge, a snow patch, rainwater, active layer groundwater, Kitluk River water and a small thermokarst lake close to the Kit-43 coring site were analysed to compare modern seasonal signals from different water sources to the isotopic composition preserved in the Kit-43 core. The δD and $\delta^{18}O$ values are given as per mil (‰) difference from Vienna Standard Mean Ocean Water (V-SMOW), with internal 1σ errors of <0.8 and <0.1‰ for δD and $\delta^{18}O$, respectively (Meyer *et al.* 2000). The deuterium excess (d excess) is calculated according to: $d = \delta D - 8\delta^{18}O$ (Dansgaard 1964) and is indicative of secondary non-equilibrium fractionation processes and conditions in the initial moisture source regions.

The gravimetric ice content was measured as the weight difference between fresh and freeze-dried bulk sediment samples and is expressed as a weight percentage (wt%). The grain-size distribution was measured with a laser particle size analyser (Coulter LS 200) according to EN ISO 14 688 after organic matter was removed with hydrogen peroxide (H_2O_2, 30%). Particles >1 mm were dry sieved through 1 and 2 mm mesh screens for 2 min (ATM Sonic Sifter) in order to differentiate the coarse sand fraction and the gravel-size clasts.

Total nitrogen (TN), total carbon (TC) and total organic carbon (TOC) were measured on bulk sediments with an elemental analyser (ElementarVario EL III; analytical accuracy of ±0.1 wt%) and the C/N-ratio (TOC/TN) was calculated. To determine the carbon stable isotope composition, $\delta^{13}C_{org}$ was analysed with a Finnigan MAT Delta-S mass spectrometer equipped with a FLASH elemental analyser and a CONFLO III gas mixing system. Values of $\delta^{13}C_{org}$ are expressed relative to the Vienna Pee Dee Belemnite (V-PDB) standard in ‰ and the standard deviation (1σ) is generally better than ±0.15‰.

Volcanic glass shards in tephra layers were identified on smear slides in glycerine and prepared for geochemical microanalysis in order to identify the source of the tephra (detailed sample preparation described in Lenz *et al.* 2016). The major element glass composition was analysed with a JEOL JXA-8230 electron microprobe with a voltage of 15 kV, a beam current of 10 nA and a beam size of 10 μm. For standardization and instrumental calibration, natural and synthetic minerals and the Lipari obsidian were used (Hunt & Hill 1996; Kuehn *et al.* 2011). To visualize the ash particles, scanning electron microscope (SEM) images were taken (Zeiss Gemini Ultra+) at the German Research Centre for Geosciences Potsdam (GFZ).

For ostracod species determination, sediment samples (sampling interval mostly 5–7 cm in core depth of 350–185 cm and 10–20 cm in core depth of 180–0 cm) with known weight normalized to 15 g of dry sediment were wet-sieved through 63 and 200 μm mesh screens, dried and examined under a stereo-microscope (Zeiss Stemi 2000-C, Carl Zeiss Microscopy GmbH, Jena, Germany). For testacean species, material was subsampled at intervals of 2–26 cm to take account of changes in sediment facies, suspended in purified water and wet-sieved through a 500-μm screen to remove organic and mineral particles. Testaceans were identified and counted in glycerine on glass slides under a light microscope at 100–400× magnifications (Zeiss Axioskop 2, Carl Zeiss Microscopy GmbH).

Ten samples were wet-sieved (>250 μm) and hand-picked to obtain macroscopic plant remains for accelerator mass spectrometry (AMS) radiocarbon dating. Three initial samples were sent to the National Ocean Sciences AMS Facility, NOSAMS (USA), and seven additional samples of plant remains, taken later to refine the chronology, were dated at the Poznań Radiocarbon Laboratory (Poland). All dates of this study shown in Table 1 are reported in calibrated radiocarbon years before present (cal. a BP) as derived from age-depth modelling with the Bacon (Bayesian accumulation histories) modelling routine in Rstudio software (Blaauw & Christen 2011; applying the calibration data set INTCAL13 according to Reimer *et al.* 2013). The age modelling method divides the sediment core into 71 sections of 5 cm thickness and estimates the accumulation rate of each section through millions of Markov chain Monte Carlo iterations. The core basal age was calibrated using CALIB 7.0 with the INTCAL13 data set (Reimer *et al.* 2013). Three additional dates from outcrops along the Lake Rhonda shoreline are reported in Table 1 for geochronological comparison.

Results

Geochronology

AMS radiocarbon dates in the Kit-43 sediment core covered the full Holocene period. Ten samples were AMS radiocarbon-dated (Table 1) and one major age inversion was identified. A sample at 310 cm, located in a reliable lithological context, consisted of sedges and higher plants mixed with aquatic plant material ($\delta^{13}C_{org}$ of −19.7‰, Table 1) and dated to 10 535±53 ^{14}C a BP. A younger age of 8890±30 ^{14}C a BP at 313 cm, immediately below the older sample,

Table 1. AMS radiocarbon age determinations from the Kit-43 core with modelled and calibrated ages derived from Calib 7.0 and the Bacon modelling routine in R (Blaauw & Christen 2011). Poz = Poznan Radiocarbon Laboratory; OS = National Ocean Sciences AMS Facility (NOSAMS); UCIAMS = UC Irvine Keck- CCAMS facility; pMC = percent modern carbon.

Lab. no.	Core depth (cm b.s.)	Dated plant material	Mass (mg C)	$\delta^{13}C_{org}$ (‰)	pMC	AMS ^{14}C age (a BP)	AMS ^{14}C age range, Calib 7.0 (cal. a BP, 2 sigma)	Bacon model age range (cal. a BP)	Bacon model median age (cal. a BP)
Kit-43									
Poz-49858	5	Remnants of roots, shoots and mosses	1.11	−31.8	153.34±0.37	−3435±19[1]	186–220	−860–359	−342.7
Poz-49859	38	Remnants of roots, *Carex*, lignified shoots, leaves of *Sphagnum* mosses	1.32	−28.0	86.12±0.28	1200±26	1182–1059	872–1125	1026
OS-83573	50	Wooden remains	n.a.	−25.8	n.a.	1160±30	1176–1045	1031–1204	1137
OS-83574	55	Bulk sedge peat	n.a.	−26.8	n.a.	1130±30	1090–962	1076–1273	1173
Poz-49861	143	Remnants of *Carex* and mosses	1.39	−25.8	64.22±0.27	3557±33	3930–2135	3668–4096	3868
Poz-49862	182	Remnants of moss and *Carex* remains	0.99	−27.3	45.6±0.23	6308±40	7317–7165	5155–7359	7007
Poz-49863	276	Remnants of shoots and mosses	0.69	−29.2	38.57±0.22	7653±45	8544–8381	8295–11 324	8788
Poz-49864	310	Remnants of *Carex* and higher plants	1.44	−19.7	26.94±0.18	10 535±53	12 689–12 379	9473–12 758	10 074
OS-83575	313	Wooden remains	n.a.	−26.7	n.a.	8890±30	10 188–9888	9715–12 818	10 138
Poz-49865	347	Non-lignified shoots and branches	1.30	−27.4	9.52±0.13	18 891±109	23 032–22 475	–	–
Kit-7									
UCIT21189	240	Wood	n.a.	−28.0	n.a.	10 375±25	12 421–12 020	Brosius *et al.* (2012)	
Kit-75									
OS-83579	112.5	Charcoal, wood	n.a.	−25.5	n.a.	8170±50	9010–9270	Jones *et al.* (2012)	
Kit-10									
UCIAMS-70597		Wood	n.a.	−24.8	n.a.	1195±15	1176–1069	Jones *et al.* (2012)	

[1]Excluded from the age model.

originated from an organic inclusion with wooden remains. Contamination with young material during the permafrost drilling process can be excluded for this sample. Accordingly, neither of the two dates could be *a priori* excluded. The samples at 38, 50 and 55 cm were of almost the same age and age inversions were negligible because they were within the range of error. The uppermost sample at 5 cm was of modern age with 153.34±0.37 percent modern carbon (pMC) and was therefore the only radiocarbon date that was manually excluded from the age model. When applying the Bacon modelling routine (Fig. 2), eight out of nine dates were situated within the 95% confidence interval; the oldest age of 18 891±109 ^{14}C a BP at 347 cm within the tephra layer was outside the likely age range. Figure 2 displays a reliable age-depth relationship for 0–182 cm but below 182 cm it shows a high discrepancy between the weighted mean (blue line) and the median (red line) of the age-depth model. In the following, the statistical median is used for applying a chronology to the Kit-43 core as it better reflects the fact that the Bacon age modelling routine considered the 8890±30 ^{14}C a BP at 313 cm to be more reliable than the 10 535±53 ^{14}C a BP at 310 cm.

The Bacon modelling routine in R calculated a basal age for the full sediment record of 12 800 cal. a BP with a mean sedimentation rate of 0.03 cm a^{-1} (with a maximum sedimentation rate of 0.05 cm a^{-1} at 276–182 cm and minimum sedimentation rate of 0.01 cm a^{-1} at 182–143 cm, Fig. 2). The basal age of the lacustrine sediment is 11 800 cal. a BP.

Cryolithological description

Based on the lithological description and analysed sedimentological, geochemical and palaeoecological parameters (Table S1), the Kit-43 permafrost core was divided into four lithostratigraphical units:

- Unit A: 350–336 cm, >11 800 cal. a BP
- Unit B: 336–283 cm, 11 800–9000 cal. a BP
- Unit C: 283–40 cm, 9000–1060 cal. a BP
- Unit D: 40–0 cm, 1060 cal. a BP–today

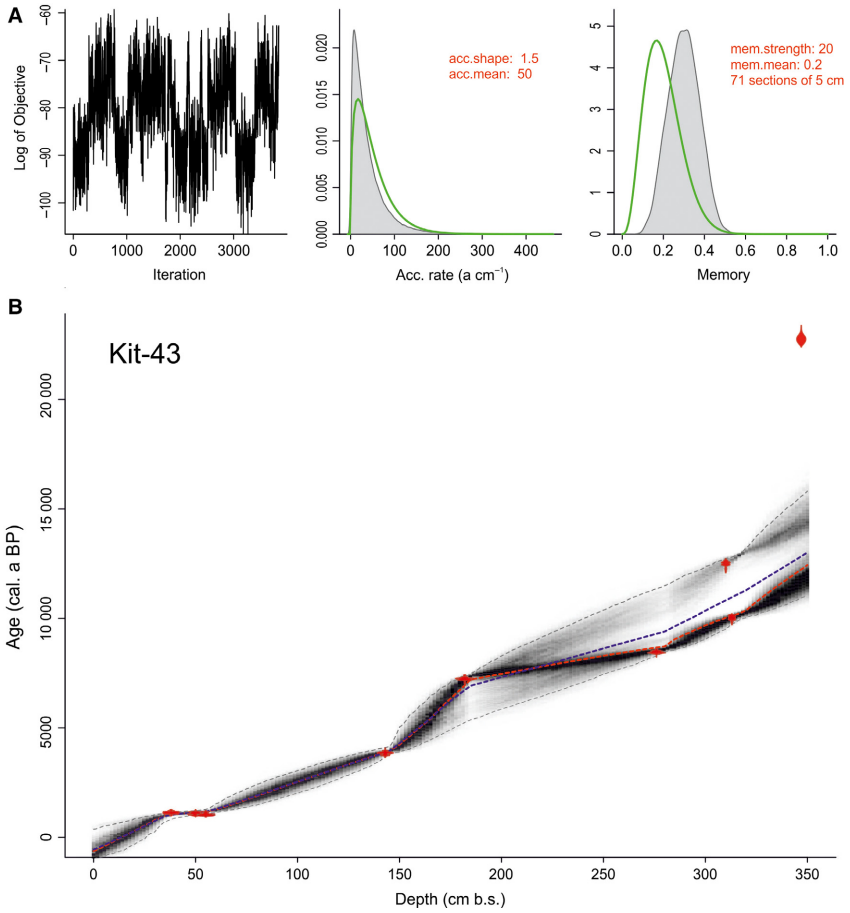

Fig. 2. Bacon modelling routine output graph of age-depth model of core Kit-43 based on radiocarbon dates (Table 1). A. Markov chain Monte Carlo iterations, prior (green curves)/posterior (grey histograms) distributions of accumulation rate and memory R of Kit-43 core. B. Calibrated radiocarbon dates (red) and age-depth model (darker greys indicate more likely calendar ages; grey dashed lines show 95% confidence intervals; blue curve shows single 'best' model based on the weighted mean age for each depth, red curve shows single 'best' model based on the median age for each depth). [Colour figure can be viewed at wileyonlinelibrary.com]

The core was mainly composed of dark olive grey (Munsell Soil Color Chart, ID 5Y 3/2) (Munsell Color Company 1994), greyish-brown (2.5YR 5/2) to dark-greyish-brown (2.5YR 3/1) fine-grained sediment. A 40-cm-thick layer of alternating poorly and well-decomposed, strong brown-to-black (7.5YR 5/6 to 2.5/1) peat characterized Unit D at the top of the core (Fig. 3). Intermediate dark-brown (7.5YR 3/2) peaty layers alternate with minerogenic deposits in Unit C whereas Unit B is characterized by more homogenous sediment deposits. Coarse-grained tephra deposits of about 14 cm thickness dominate Unit A at the base of the core from 350 to 336 cm as well as different overlying sections; these observations were also supported by grain-size analyses. Whereas Unit B and C are dominated by silt with varying proportions of clay and sand, coarse sand and gravel-size clasts up to 5 mm characterize tephra layers in Unit A and deposits at 239–226, 202–178 and 163–138 cm (Fig. 4). The coarse grain size and described tephra deposits in Unit A are also reflected in the sediment core MS (Fig. 4). MS increased down-core from 0 (within the first metre from the top; Unit D and part of Unit C) to 47 at 335 cm with high values up to 88 in Unit A and pronounced peaks of 192 at 238–228 cm and 140 at 200–192 cm within Unit C where tephra layers were identified.

Following French & Shur (2010), the cryostructure of Kit-43 was characterized as predominantly structureless below 156 cm (Unit A, B and part of Unit C), whereas ice lenses up to 5 mm thick, ice veins up to 10 mm thick, and wavy parallel lenticular layers were prevalent in the upper part from 156 to 0 cm (Unit D and part of Unit C); transparent ice structures with bubbles were noted in Unit C at 88–87 and 74–66 cm (Fig. 3). The gravimetric ice content ranged from 77.7 wt% at 70–69 cm in Unit C to 8.8 wt% at the core bottom (Unit A) with a decreasing trend down-core, although stable values around 26 wt% were measured between 343 and 282 cm in Unit B (Fig. 4).

Geochemical results

All geochemical analysis results are displayed in Fig. 4. The average TN of Kit-43 core sediments was 0.59%. TN was below detection limits in layers described as tephra (in Unit A) and was highest in the terrestrial surface peat (Unit D). A TN_{Max} of 2.4% occurred within Unit D at 35–34 cm. Average TC was 11.1%; TC_{Min} of 0.4% was found in Unit A and in tephra layers in Unit C, and the highest TC values occurred within the peat in Unit D (TC_{Max} of 44% at 35–34 cm). TOC followed a similar pattern, with a TOC_{Min} of 0.2% in tephra layers (Unit A and parts of Unit C), the highest TOC in the terrestrial surface peat in Unit D (TOC_{Max} of 40% at 35–34 cm), and an average core TOC of 10%. The C/N ratio generally decreased down-core from about 30–2. Values of

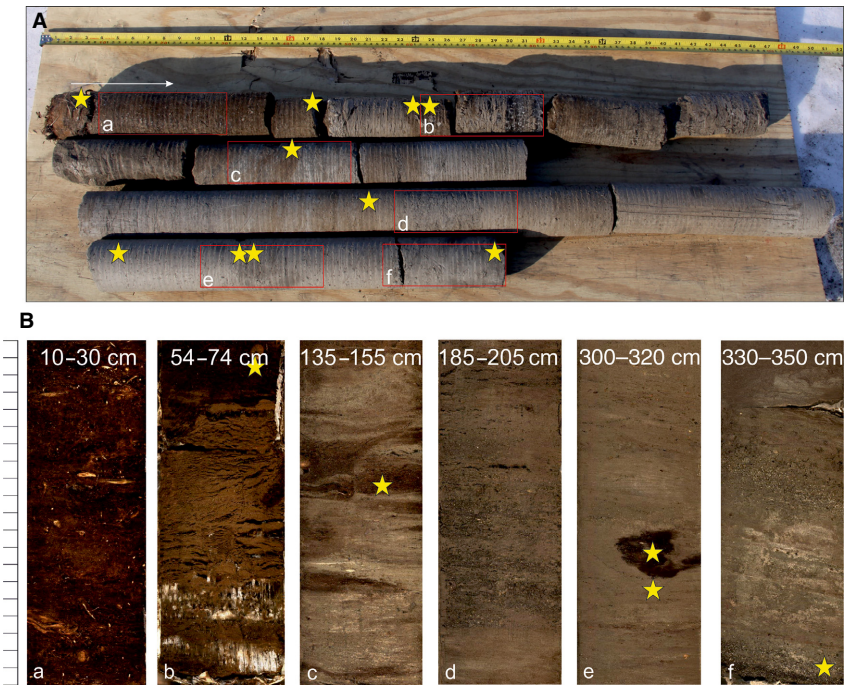

Fig. 3. A. Core Kit-43 as recovered in the field in April 2009; yellow stars mark radiocarbon samples, core segments from left (top) to right (bottom). B. Close-up of high-resolution photographs of different sections; vertical scale is cm. [Colour figure can be viewed at wileyonlinelibrary.com]

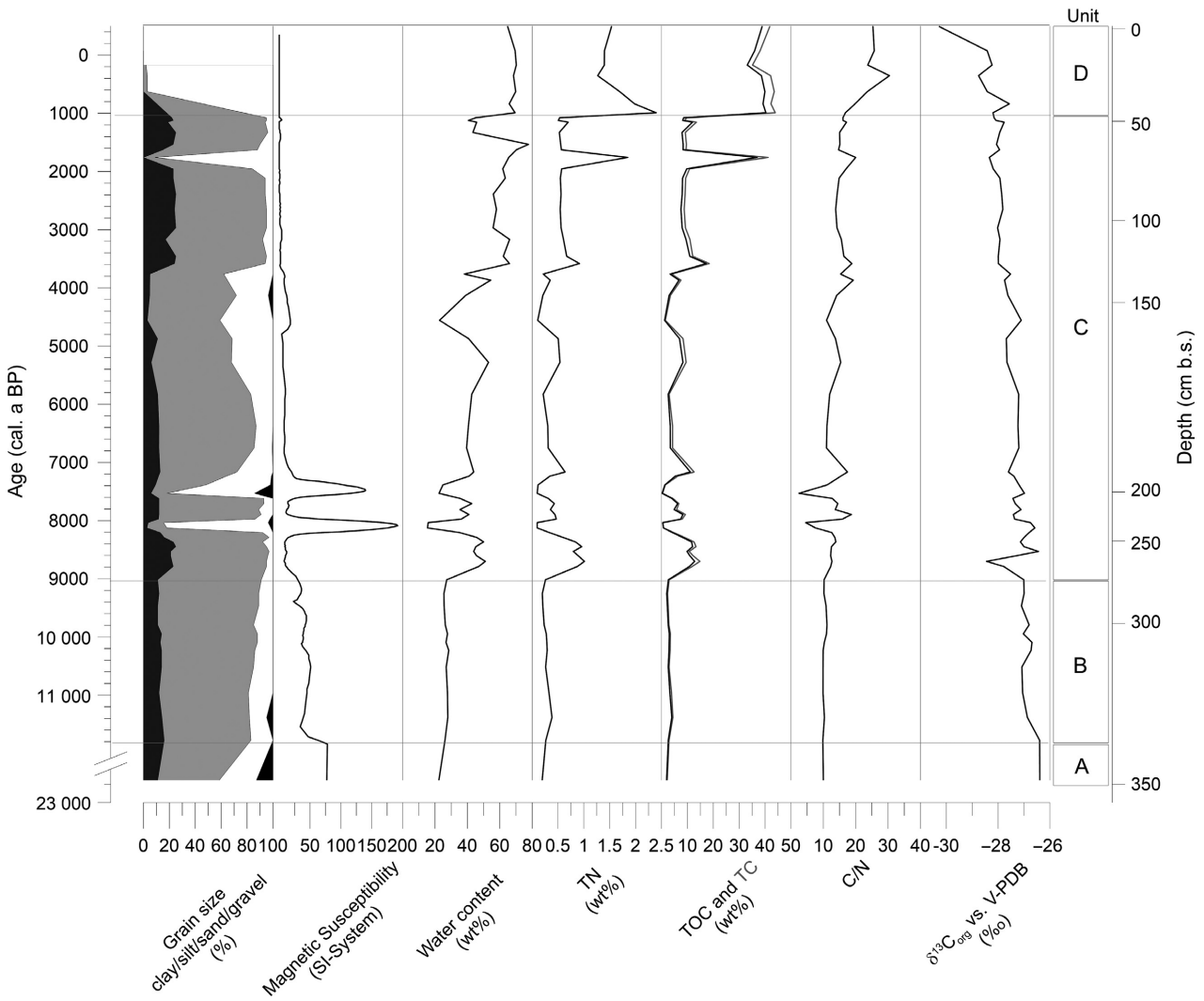

Fig. 4. Lithological and geochemical results of core Kit-43 according to calibrated and modelled ^{14}C ages: grain size, magnetic susceptibility, water content, total nitrogen (TN), total carbon (TC, in grey), total organic carbon (TOC), C/N ratio and $\delta^{13}C_{org}$ vs. V-PDB (proxy values are given in Table S1).

$\delta^{13}C_{org}$ increased core-downwards from −30.3 to −26.5‰ (−27.5‰ on average); a pronounced negative peak of −28.45‰ was measured at 271–270 cm in Unit C.

Tephra analyses of 24 and 23 glass shards at depths of 349–348 cm (Unit A) and 201–200 cm (Unit C), respectively, yielded similar geochemical compositions. These values were similar to results obtained from tephra at a depth of 243–155 cm from the Kit-64 core of a drained lake basin (Lenz *et al.* 2016) and tephra found in a nearby pingo outcrop (Wetterich *et al.* 2012) (Table 2, Table S2). SEM images visually showed rather sharp tephra particles at the depth of 349–348 cm in Unit A compared to rounded particles at the depth of 201–200 cm in Unit C (Fig. 5).

Bioindicators

Three species of ostracods were identified in 47 Kit-43 core samples (Fig. 6). *Cypria ophtalmica* was identified in all samples where ostracods were present, except for one sample at 3–2 cm depth in Unit D. Here, a single carapace of *Candona elliptica* was identified. *Cyclocypris ampla* was identified in Unit A at depths of 339–338 cm, as well as in Unit B at 332–331, 323–321 and 294–276 cm depth; a single carapace was found at the depth of 159–158 cm in Unit C. Specimen counts per sample varied from single finds up to a maximum of 234 valves (*Cypria ophtalmica*) at 271–270 cm in Unit C. Ostracods were absent in layers where tephra was noted (i.e. 350–343, 237–231 and 202–194 cm), but two

Table 2. Electron probe analyses of glass shards from different tephra samples from the Seward Peninsula. Data are expressed as normalized mean (volatile-free) values (wt%), number of single glass shards analysed and their standard deviations (SD). Single non-normalized data of all samples and the Lipari obsidian reference standard are given in Table S2.

Sample	SiO_2	TiO_2	Al_2O_3	FeO	MnO	MgO	CaO	Na_2O	K_2O	P_2O_5	Total	Cl	F
Kit-43, 201–200 cm	51.08	2.57	15.12	10.17	0.15	5.95	9.57	3.74	1.18	0.45	100.01	0.04	0.00
SD (n = 23)	0.42	0.52	0.02	0.49	0.25	0.31	0.27	0.10	0.42	0.52		0.02	0.01
Kit-43, 349–348 cm	51.39	2.47	15.01	10.11	0.16	6.16	9.61	3.58	1.09	0.39	100.01	0.04	0.00
SD (n = 24)	0.42	0.40	0.02	0.50	0.44	0.15	0.17	0.05	0.42	0.40		0.04	0.00
Kit-64, 243–155 cm	51.20	2.66	15.30	9.86	0.15	5.61	9.38	3.89	1.41	0.51	100.01	0.04	0.00
SD (n = 8)	0.73	0.14	0.28	0.11	0.01	0.23	0.21	0.12	0.08	0.04		0.01	0.00
Kit-1, 6 cm (Pingo)	51.22	2.81	14.95	10.06	0.16	5.39	9.66	3.88	1.35	0.50	100.01	0.03	0.00
SD (n = 24)	0.23	0.17	0.39	0.44	0.02	0.36	0.34	0.15	0.35	0.04		0.01	0.01
Kit-1, 13 cm (Pingo)	51.05	2.48	15.21	10.52	0.17	5.70	9.72	3.60	1.19	0.04	100.09	0.40	0.00
SD (n = 24)	0.51	0.18	0.28	0.42	0.02	0.47	0.39	0.19	0.17	0.02		0.05	0.00

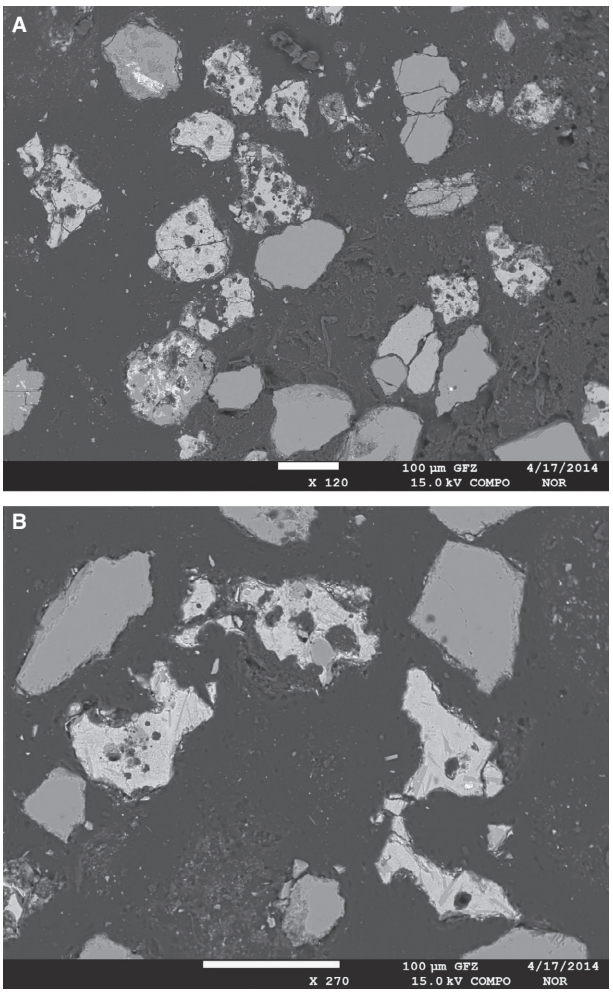

Fig. 5. SEM images of polished tephra grains in resin. A. Tephra particles at 120× magnification found at 200–201 cm core depth. B. Tephra particles at 270× magnification found at 348–349 cm core depth.

ostracod valves were documented within the tephra layer at 339–338 and 337–336 cm in Unit A.

A total of 34 samples was analysed for testaceans (Fig. 6). Eleven samples did not contain any testaceans and 23 samples yielded 56 testacean taxa including subspecies and varieties of 15 genera. Specimen counts per sample varied from single finds to 47 counts per sample in the surface peat layer of Unit D. Higher specimen counts correlated positively with a larger number of ecological groups in the core. Whereas varying proportions of eurybiontic species (tolerating a wide range of a particular environmental factor, e.g. pH or soil moisture) and hygrophilous species (indicating moist habitats) were present in the core, sphagnobiontic species (typical inhabitants of *Sphagnum* moss) were present throughout Unit C and Unit D. Hydrophilous species, indicating waterlogged habitats, were only documented at depths of 306–305 and 256–255 cm (Unit B), 158–157 cm (Unit C) and at the top at 2–1 cm (Unit D).

Characteristics of intra-sedimentary ice and comparison with modern waters

The isotopic composition of intra-sedimentary ice allows us to distinguish five hydrological units in the Kit-43 core that are independent of the lithostratigraphical units described above because they represent the post-drainage hydrology and freezing at the study site:

- Hydrological Unit I: 0–42 cm
- Hydrological Unit II: 42–82 cm
- Hydrological Unit III: 82–154 cm
- Hydrological Unit IV: 154–343 cm
- Hydrological Unit V: 343–350 cm

The isotopic composition of the intra-sedimentary ice from the Kit-43 core ranged between −13.9 and −10.6‰ for $\delta^{18}O$ and from −108.6 to −83.8‰ for δD. A pronounced heavier isotopic composition was observed at 349–348 cm (Hydrological Unit V; $\delta^{18}O = -11.6‰$ and $\delta D = -92.3‰$), at 70–69 cm ($\delta^{18}O = -10.6‰$ and $\delta D = -86.2‰$) and at 42–41 cm (transition between Hydrological Units I and II; $\delta^{18}O = -11.8‰$ and $\delta D = -90.9‰$). The d excess varied from −2.3 to +8.1‰ and reached its lowest levels at the $\delta^{18}O$ maxima. In general, the isotopic composition was more variable in the upper part of the core

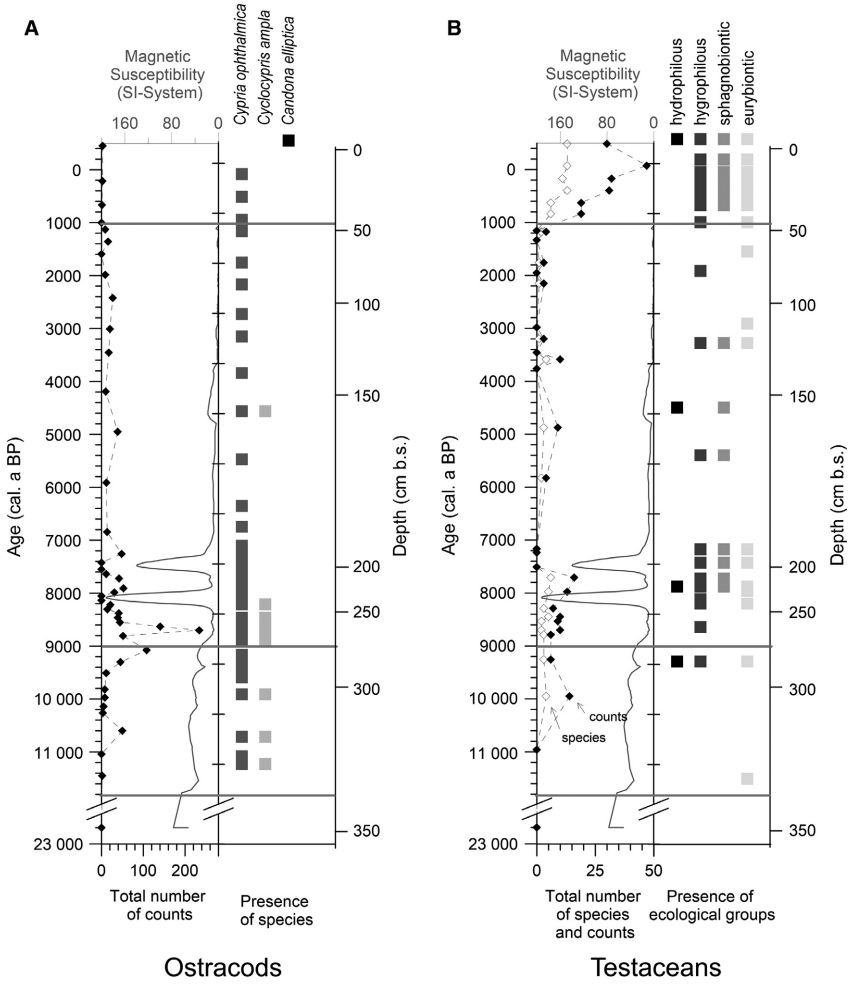

Fig. 6. A. Ostracod individual counts and species. B. Testacean individual counts, number of species, and ecological groups. Both graphs also show magnetic susceptibility as an indicator of tephra layers in the Kit-43 core.

(Hydrological Units I, II, III) and became more stable from 154 cm down-core (Hydrological Unit IV).

Furthermore, to compare past and modern isotopic characteristics of pore waters in the core and from the surrounding landscapes, six types of waters were analysed (Table 3). Isotope data from groundwater in the modern active layer as well as samples from open waters, such as from the Kitluk River, are similar to Kit-43.

Discussion

The analytical results from the Kit-43 sediment core are used to reconstruct the evolution of a thermokarst lake system on the northern Seward Peninsula of Alaska extending from 11 800 cal. a BP to present. The application of an age-depth-model allows the determination of the timing of sediment facies changes associated with past landscape dynamics. The magnetic susceptibility of the sediment record reflects changes in grain size or content of magnetic minerals and therefore indicates input of allochthonous material into the lake (Thompson *et al.* 1975), which is most likely to be tephra in the Kit-43 record. The tephra layers in core Kit-43 were geochemically analysed for comparison with tephra in other studies and to estimate its value as a chronostratigraphical marker. The geochemical proxies of TN and TC indicate nutrient supply and past bioproductivity in the lake (Cohen 2003; Lamoureux & Gilbert 2004) whereas TOC content gives a signal for autochthonous productivity and for allochthonous organic input into the lake system (Lamoureux & Gilbert 2004). The TOC content is probably also related to the magnitude of decomposition of organic matter in unfrozen lake sediments, in which older layers had more time to decompose and thus should be depleted in TOC relative to younger lake sediments. The C/N ratio can be used as an indicator of different states of mineralization of organic matter in core Kit-43 and in combination with $\delta^{13}C_{org}$ it may be used to discriminate organic matter sources (Meyers 1997; Meyers & Takemura 1997).

Table 3. Isotope composition of intra-sedimentary ice in permafrost core Kit-43 compared to modern waters.

Type of sample		$\delta^{18}O$ (‰)	δD (‰)	d excess (‰)
Lake water	n = 2	−9.20	−80.9	−7.3
(modern surface water)	SD	0.01	0.01	0.1
Kitluk River	n = 2	−12.08	−99.1	−2.4
(modern surface water)	SD	0.03	0.12	0.13
Rain water	n = 12	−15.61	−127.5	−2.6
(modern summer precipitation)	SD	2.9	17.7	6.5
Active layer water	n = 4	−14.74	−109.6	+8.3
(modern groundwater)	SD	0.4	1.9	1.4
Snow patch	n = 20	−20.89	−161.2	+5.9
(modern winter precipitation)	SD	0.7	4.8	1.0
Ice wedge	n = 38	−23.80	−183.5	+6.8
(past winter precipitation)	SD	0.6	5.9	2.9
Kit-43				
Hydrological	n = 8	−12.31	−92.7	5.9
Unit I (0–42 cm)	SD	0.6	4.0	1.5
Hydrological	n = 7	−12.17	−95.9	1.5
Unit II (42–82 cm)	SD	0.8	4.7	2.4
Hydrological	n = 11	−13.46	−106.2	1.5
Unit III (82–154 cm)	SD	0.4	2.4	1.2
Hydrological	n = 37	−13.04	−104.5	−0.2
Unit IV (154–343 cm)	SD	0.2	1.0	1.0
Hydrological	n = 1	−11.64	−92.3	0.8
Unit V (343–350 cm)				

Palaeoecological analyses of ostracods and testaceans were able to differentiate lake stages and terrestrial phases, and to describe past ecological conditions. Finally, the isotopic composition of the intra-sedimentary ice reflects the situation after the drainage of Mama Rhonda Lake and, in comparison to modern waters, allows study of the changes in permafrost conditions after drainage. Our interpretations of lake stages and associated landscape changes based on all analysed proxies are described in detail below and a conceptual schematic is presented in Fig. 7.

Thermokarst lake dynamics

Pre-lake environment: >11 800 cal. a BP (Unit A). – Ice-rich permafrost was present prior to lake formation at the study site. The Bering Land Bridge tundra was drier than present during the Lateglacial, and fossil insect remains indicate an arctic climate (Elias *et al.* 1997). A cold permafrost environment of at least −8 to −6 °C mean annual air temperature or colder was reconstructed for the LGM from ice wedges underlying the Kitluk palaeosol as well as from blocky soil structures indicating the formation of ice nets and ice lenses within the palaeosol (Washburn 1980; Höfle *et al.* 2000). A chronology for the Devil Mountain Maar tephra was established using radiocarbon dates from the Kitluk palaeosol. The Devil Mountain Maar eruption occurred around 18 000 ^{14}C a BP (21 500 cal. a BP) and covered about 2500 km^2 of the northern Seward Peninsula with a tephra layer of varying thickness (Begét *et al.* 1996). Two radiocarbon dates have been published for the tephra originating from a Lake Rhonda bluff outcrop: 17 420±260 ^{14}C a BP (Begét *et al.* 1996) and 19 630±110 ^{14}C a BP (Höfle *et al.* 2000).

The tephra layer at the base of the Kit-43 core was dated to 18 891±109 ^{14}C a BP (22 800±280 cal. a BP) and is in chronological agreement with the Devil Mountain Maar tephra. Thus, the results from this study align well with the existing chronology of landscape evolution in this region. The geochemical composition of the tephra layer is very similar to that of the much older South Killeak Maar tephra detected 19 km to the southeast in the Kit-64 drained lake basin core (Lenz *et al.* 2016; Fig. 1) and in the Kit-1 pingo outcrop east of the Rhonda basins (Wetterich *et al.* 2012; Fig. 1, Table 2). We argue that the geochemical similarity of these different tephra layers with their evidently different ages is due to these phreatomagmatic maar eruptions originating in the same geological setting of the Cape Espenberg maars and thus producing very similar geochemical signatures.

Subsequent thermokarst lake formation in ice-rich permafrost resulted in a vertical displacement of tephra in Unit A during thaw subsidence. As illustrated in Fig. 7B there is a more than 15 m elevation difference between *in situ* Devil Mountain Maar tephra in the adjacent yedoma upland vs. the tephra in Unit A of core Kit-43. Although substantial horizontal transport processes can be ruled out because the tephra particles evidently are still characterized by sharp edges (Fig. 5), thaw subsidence and compaction influenced the stratigraphical bedding of terrestrial deposits including the tephra layer during lake formation.

Lake development (Grandma Rhonda lake phase): c. 11 800–9000 cal. a BP (Unit B). – Lacustrine sediment accumulated on top of terrestrial deposits, as is clearly indicated by a sedimentological change to silty deposits and the occurrence of the two ostracod species *Cypria ophtalmica* and *Cyclocypris ampla*. Little variability in geochemical parameters in Unit B suggests that the coring location was distant from a dynamic shoreline of a large water body. This is supported by grain-size analyses that show a decrease in the sand and increase in the silt fraction from 11 800 to 9000 cal. a BP. Decreasing MS indicates a lower input of tephra from eroding shores, thus indicating that the lake area expanded or the lake deepened such that the core site was deeper than the wave base. According to the age-depth model, the initiation of the studied lake basin was at about 11 800 cal. a BP. This coincides with the end of the Younger Dryas (*c.* 12 800–11 500 cal. a BP, Kokorowski *et al.* 2008; Kaufman *et al.* 2010), which was triggered by changes

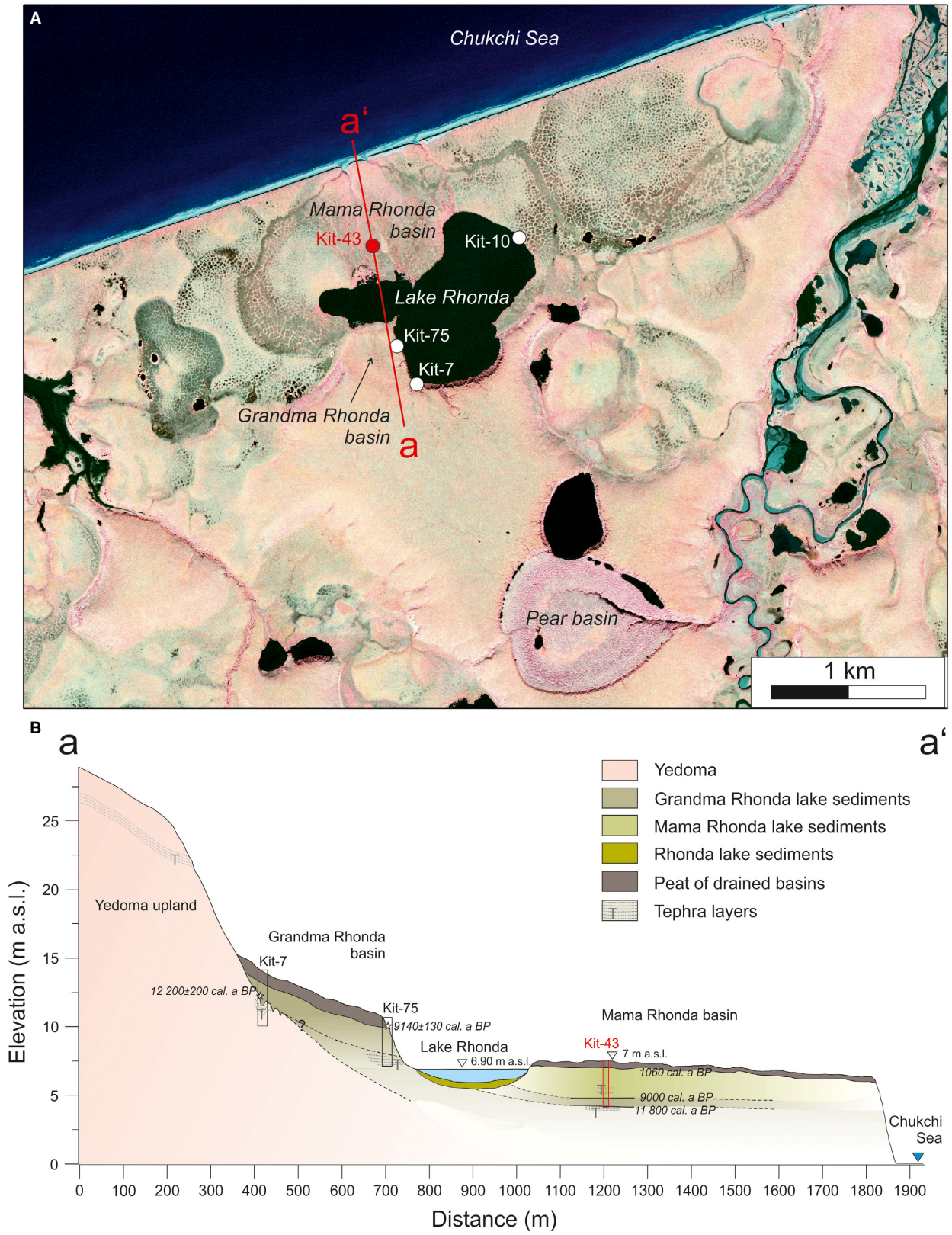

Fig. 7. A. Spot satellite image (©SpotImage) of the study region and B. cross-section of Mama Rhonda basin and neighbouring Grandma Rhonda basin and Lake Rhonda. Surface elevations along the cross-section were derived from a high-resolution digital elevation model. Dashed lines give the hypothetical extent of sediment packages. Chronological correlations described in the text are noted in outcrops at the shore of Lake Rhonda. Note the strong height exaggeration of the cross-section. [Colour figure can be viewed at wileyonlinelibrary.com]

in ocean-water circulation in the North Atlantic and showed spatially complex palaeoclimatic patterns (Kokorowski *et al.* 2008). Whereas southern Alaska seems to have been very susceptible to changes in atmospheric circulations, some studies have also recorded simultaneous cooling in northern Alaska (e.g. Mann *et al.* 2010; Meyer *et al.* 2010). For interior Alaska, several studies have suggested uniform climate or even warming during the Younger Dryas (Kokorowski *et al.* 2008). Bigelow & Edwards (2001) observed a shift from low lake levels and sparse herbaceous tundra vegetation to higher lake levels and shrub tundra around 11 800 ^{14}C a BP (*c.* 13 600 cal. a BP) in eastern Beringia. On the southern part of the Seward Peninsula, in turn, Hunt *et al.* (2013) reported the presence of *Picea* spp. and *Larix laricinia* in peatlands from 13 500 to 12 100 cal. a BP, indicating a warm regional climate, followed by a cold and dry interval from 12 100 to 11 100 cal. a BP. The Younger Dryas seemed to be absent in records from e.g. Imuruk Lake (Colinvaux 1964) and Cape Deceit (Matthews 1974). Kaufman *et al.* (2004) summarized an interval of warmer-than-present Holocene temperatures in Alaska between 11 500 and 9000 cal. a BP with an initiation of the Holocene Thermal Maximum (HTM) in central-eastern Beringia at 11 300±1500 cal. a BP but also highlighted the complex spatial pattern of highly variable temperature during that time (Kaufman *et al.* in press).

Our sediment core records the early onset of thermokarst dynamics at the Lateglacial to Holocene transition during a time when the Bering Land Bridge was rapidly narrowing. By 11 000 cal. a BP the Land Bridge was closed due to postglacial sea-level rise and the June and July solar insolation started to reach its maxima at 65°N latitude (Elias 2001). The Kit-43 record captures the initial landscape shifts from a continental-climate-dominated accumulation plain to a warming and wetter environment under increasing maritime influence. At the same time, model simulations of thermokarst lakes on the northern Seward Peninsula demonstrate that lake expansion is not necessarily climate-driven but is strongly related to topography (Kessler *et al.* 2012). As the HTM was not yet fully developed during lake initiation and early lake development, stable shoreline slope conditions may have contributed to the development of a surprisingly stable lake system at the Kit-43 site.

Radiocarbon ages from outcrops along the shore of Lake Rhonda provide additional context for the chronological relationship of lake generations. A radiocarbon age (Table 1) of an ice-wedge cast (Kit-7, Fig. 7) containing basal lake sediments suggests that the associated lake basin (informal name: Grandma Rhonda lake basin) initiated around 12 200±200 cal. a BP. Considering the large error of 200 years for the Kit-7 date and wide 95% confidence interval ranging from 10 500 to 14 700 (with the median at 11 800) cal. a BP for this time period in the age-depth model of Kit-43 (Fig. 2), it is possible that the initiation of the first lake generation detected in Kit-43 coincides with the initiation of Grandma Rhonda lake. As the Grandma Rhonda lake site at Kit-7 and the Kit-43 site are <800 m apart, these older deposits in both records may thus well belong to the same lake system (Fig. 7); hence, we term this lake phase the 'Grandma Rhonda lake phase'. Furthermore, there is geochronological evidence that not only Grandma Rhonda lake initiation (transition Unit A/B) is preserved in the Kit-43 core, but also Grandma Rhonda lake drainage. According to the nearby Kit-75 exposure (Fig. 7), which preserves at least 160 cm of lake sediments with reworked tephra deposits overlain by 112.5 cm of terrestrial peat (G. Grosse, unpublished data), the Grandma Rhonda lake drainage was radiocarbon dated in Kit-75 to 9140±130 cal. a BP (Jones *et al.* 2012). At about the same time at 9000 cal. a BP, core Kit-43 shows a drastic transition from stable proxies to strongly variable proxies (TN, TC, TOC, water content, and even testacean and ostracod counts; see below). Due to the spatial closeness of these sites it is very likely that the drainage event recorded in Kit-75 is coincident with the event causing the depositional change in our core. We suggest that the first generation of Grandma Rhonda lake either did not drain completely or that a second lake generation rapidly developed at the study site.

Lake modification (Mama Rhonda lake phase): c. 9000–1060 cal. a BP (Unit C). – An abrupt change of facies was detected in core Kit-43 at around 9000 cal. a BP. Here, all geochemical proxies become more variable than in Unit B, pointing towards an alternating lake level with the potential for intermediate wetland development; the generally increased contents of nitrogen, carbon (in particular organic carbon) and water in the sediments indicate a higher input of organic matter. In addition, the average C/N ratio in Kit-43 is elevated from 10.4 in Unit B to 14.6 in Unit C (excluding tephra layers with extremely low TN, TC and TOC contents), pointing towards enhanced input of terrestrial matter due to shoreline erosion. The maximum Unit A ostracod count at 8700 cal. a BP, dominated by the cosmopolitan species *Cypria ophtalmica*, indicates optimal ecological conditions in a large but generally shallow freshwater lake at the beginning of the Mama Rhonda lake phase.

Pronounced peaks in MS, coarse grain-size fractions and a change in geochemical parameters at about 230 and 200 cm depth, as well as a high sedimentation rate of 0.053 cm a^{-1} at 276–182 cm, indicate rapid input of tephra from the catchment. The tephra particles are of the same geochemical composition as the tephra at the core base (Table 2) but no volcanic eruption in the

Cape Espenberg lowland area is known after the Devil Mountain Maar eruption around 21 500 cal. a BP (Begét *et al.* 1996). The tephra in Unit C is most probably reworked because the particles are more rounded than the tephra particles at the core base, which subsided vertically in place (Unit A), suggesting at least some horizontal aquatic transport of sediments in Unit C (Fig. 5). Such a dynamic ecosystem implies unfavourable living conditions for aquatic organisms such as ostracods, which have a variable abundance in this unit (Fig. 6). Absence of ostracods gives evidence for rapid transportation and deposition of tephra particles. The low occurrence of testaceans as a general terrestrial indicator (with varying proportions of hydro- and hygrophilous as well as sphagno- and eurybiontic species throughout the core; Fig. 6) points towards a dynamic depositional environment but possibly also intermediate wetland development in the catchment and input of peaty deposits from shore erosion.

Mama Rhonda lake probably started as a small residual lake of Grandma Rhonda lake that gradually grew and persisted with oscillating lake levels over much of the Holocene. Kaufman *et al.* (in press) summarized that lake levels were consistently lower during the early Holocene and started to raise around 9000 cal. a BP in northern and interior Alaska. During that time re-organization of the periglacial landscape may have been a result of rapidly expanding thermokarst lakes. Coalescence with other remnant lakes would have caused renewed sediment input and changing lake levels that, in turn, caused the observed high variability of lithological and geochemical proxies in the Kit-43 core. Remnant lakes in the centre or on the margins of drained lake basins have been frequently observed in the study region (e.g. Hopkins & Kidd 1988; Jorgenson & Shur 2007; Jones *et al.* 2011; Lenz *et al.* 2016). Additionally, new lakes may form following complete drainage along basin margins where sufficient ground ice is still available, as well as in the centre of a basin following sufficient accumulation of post-drainage ground ice (Jorgenson & Shur 2007; Jones *et al.* 2011). A similar setting can be observed in Pear basin, a large, deep, drained lake basin about 2 km south of Lake Rhonda (Fig. 7).

For the second lake phase (Mama Rhonda lake), the period of more than 8000 years seems to be rather long for persistence of a thermokarst lake on the northern Seward Peninsula. It is possible that several lake cycles are represented by Unit C. Even if they are not clearly identifiable in the sediment core, they might be indicated by changes in sedimentation rate e.g. at 8700, 7000 and/or 3900 cal. a BP (Fig. 2). Another possibility for Mama Rhonda lake is that it developed rather slowly after the HTM with ongoing Holocene cooling and drying. Hopkins & Kidd (1988) suggested that the life span of thermokarst lakes on the northern Seward Peninsula is typically as short as 2500–3000 years but that larger lakes may persist for 4000–5000 years. In environments with deep ground ice (>20 m), like the northern Seward Peninsula, basins of >100 m diameter and depths of about 20 m may form in *c.* 5000 years (West & Plug 2008), but also as rapidly as in 300 years (Lenz *et al.* 2016). If Mama Rhonda lake did not comprise several lake phases, it would have been one of the exceptional old lakes before it drained. The longevity of this lake phase may be explained by a general cooling trend throughout the Holocene (Kaufman *et al.* 2004). Old thermokarst lakes are known e.g. in the Northwest Territories, Canada: the prominent experimental Lake Illisarvik initiated about 9500 cal. a BP (with maximum lake expansion at 6000 cal. a BP and shrinkage to its pre-drainage size by 2000 cal. a BP; Michel *et al.* 1989) before it was artificially drained in AD 1978 (Mackay 1997). In the Yukon Flats upland, deep thermokarst lakes also prevailed throughout the Holocene (Edwards *et al.* in press).

Lake drainage (Mama Rhonda drained thermokarst lake basin phase): c. 1060 cal. a BP to present (Unit D). – Finally, in the late Holocene, Mama Rhonda lake drained at about 1060 cal. a BP, as indicated by the abrupt transition from lacustrine sedimentation to a terrestrial peat. The number of testacean counts significantly increased to 47 individuals per sample, dominated by mainly hygrophilous and sphagnobiontic species. Hydrophilous testacea dominate only at 2–1 cm, indicating modern summer water-logged conditions. Occasional occurrences of the ostracod species *Cypria ophtalmica* at 27–26 and 17–16 cm and the unique presence of *Candona elliptica* at 3–2 cm were noted for this predominantly terrestrial phase of thermokarst basin development.

The drainage of Mama Rhonda coincides with the Medieval Warm Period, which previously has been connected to increased aeolian activity and dune expansion from 1050 to 550 cal. a BP in northwest Alaska (Mann *et al.* 2002b). Mann *et al.* (2002b) concluded that dune expansion in the Kobuk valley was primarily controlled by the regional moisture balance, which, in turn, is most probably related to late-summer storms. In the case of Mama Rhonda lake, summer storms could have enhanced wave activity on the lake as well as lake shore and coastal erosion, which then may have triggered the drainage event. A basal peat age of 1125±50 cal. a BP (Kit-10, Table 1) <1 km east of the study site (Fig. 7) indicates coinciding drainage events in the vicinity, which probably would have affected the local hydrological regime in the surroundings of the Kit-43 site.

The isotopic compositions of intra-sedimentary ice as well as river and lake waters cluster in the heavy part of the $\delta^{18}O$-δD diagram. Kit-43 samples taken in April 2009 display similar, but slightly heavier isotope compositions relative to rainwater, representing the

modern summer signal. In contrast, the isotopic signatures of a snow patch and an ice wedge in the study area are lighter (more negative) and both represent a winter signal (Fig. 8). Kit-43 intra-sedimentary ice samples plot slightly below the Local Meteoric Water Line (LMWL, $\delta D = 7\delta^{18}O\text{-}11$) of Barrow (Fig. 8B), which indicates some alteration of the isotope composition by secondary fractionation processes (i.e. evaporative enrichment) compared to local modern winter and summer signals; these palaeo-winter signals both correspond well with the LMWL and Global Meteoric Water Line ($\delta D = 8\delta^{18}O + 10$; Craig 1961). The Kit-43 samples from the sediment surface down to 42 cm represent the modern active layer (with a slope of 6.2 in the co-isotope plot). The position of these sample series in the co-isotope plot (Fig. 8B) indicates that the active layer has been saturated by summer precipitation rather than by snow-melt. A similar pattern is noticeable at 82–42 cm with a slightly lower d excess (slope of 5.7). Based on these very similar patterns we assume that the position of a palaeo-active layer related to the period prior to peat formation is preserved. After the lake drained at 1060 cal. a BP, and before the peat accumulated on top of the drained lake sediment surface, the terrain surface was probably in direct atmospheric exchange.

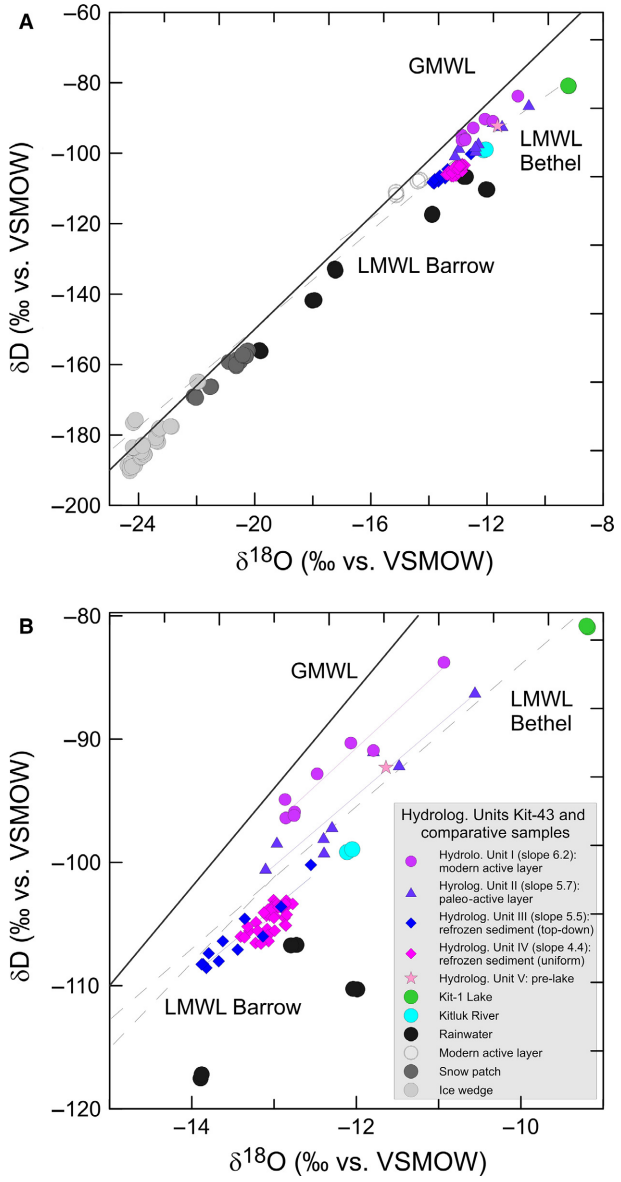

Fig. 8. A. $\delta^{18}O$-δD diagram of samples from permafrost core Kit-43 (in purple) compared to different types of ice and water (in grey, blue and green). B. Close-up of same diagram with focus on Kit-43 core samples. GMWL = global meteoric water line; LMWL = local meteoric water line for Barrow and Bethel (http://www-nawe-b.iaea.org/napc/ih/IHS_resources_gnip.html). [Colour figure can be viewed at wileyonlinelibrary.com]

The difference in the isotopic composition of the modern and palaeo-active layers suggests a change in the active layer dynamics and characteristics due to build-up of a post-drainage peat layer. Heavy hydrogen and oxygen isotope compositions and low d excess are visible at the boundary between the modern and palaeo-active layers and the permafrost table where water migrated toward the freezing front (first ice during fractional freezing). Below 82 cm, the trend from heavy to lighter isotopic composition indicates that the talik refroze from top to bottom. Below 154 cm, intra-sedimentary ice was described as structureless and oxygen isotope values and d excess were relatively uniform at −13 and 0‰, respectively. This points to a uniform water source (i.e. the adjacent lake) and no significant secondary isotope fractionation processes related to evaporation and/or melting/freezing. A similar situation has been found near Lake El'gygytgyn, where lateral contact with the adjacent lake and open system freezing have been suggested to explain uniform isotope composition over large parts of a permafrost core (Schwamborn *et al.* 2014). Hence, we assume a complex talik system next to our coring location due to the presence of Lake Rhonda until the present time.

Regional lake dynamics and global environmental change

From lake initiation in the Lateglacial at 11 800 cal. a BP to final drainage in the late Holocene at 1060 cal. a BP, different lake generations were archived in the Kit-43 core. Superimposed sets of thermokarst lake generations were previously assumed on the northern Seward Peninsula based on field observations and remote sensing. Hopkins & Kidd (1988) described sediment sequences in exposures with up to three thermokarst generations; Jones *et al.* (2012) detected assemblages of up to six partially overlapping lake generations with remote-sensing studies. Wetterich *et al.* (2012) investigated a pingo exposure (Kit-1, about 10 km east of Kit-43) and found cyclic permafrost aggradation and degradation over stadial–interstadial

and glacial–interglacial time periods. At Kit-1, following a late mid-Wisconsin thermokarst lake, polygonal shallow water deposits were described for the late Wisconsin, before a thermokarst lake re-initiated in the early Holocene around 9400 cal. a BP and drained again in the mid-Holocene. The early Holocene lake formation in Kit-1 therefore nearly overlaps with the transition from the Grandma Rhonda lake phase to the Mama Rhonda lake phase shown in Kit-43 at 9000 cal. a BP, which also corresponds with the end of the HTM on the Seward Peninsula (Kaufman *et al.* 2004) and rising lake levels in interior and northern Alaska (Kaufman *et al.* in press).

Regional thermokarst lake formation in the Lateglacial and early Holocene may have been predominantly caused by a warming and wetter climate. Such trends are indicated by a variety of evidence: invasion of *Populus* (Nelson & Carter 1987; Mann *et al.* 2002a; Ager 2003), occurrence of fossil beaver dams and beaver-gnawed wood beyond the modern presence of beavers (McCulloch & Hopkins 1966; Hopkins *et al.* 1981; Kaufman & Hopkins 1985) and buried ice-wedge casts on the Seward Peninsula (McCulloch & Hopkins 1966), as well as increased shrub cover, paludification of the landscape in northern Alaska (Detterman 1970; Oswald *et al.* 1999; Mann *et al.* 2002a, 2010; Jones & Yu 2010; Hunt *et al.* 2013) and fossil beetle assemblages indicative of climate amelioration (Nelson & Carter 1987; Elias 2000); all of these proxies indicate increased moisture availability and warmer-than-present temperatures in northwestern and northern Alaska during that time. Climate models suggest that warm and moist air masses coming from the North Pacific (Bartlein *et al.* 1998) were responsible for rising lake levels (Edwards *et al.* 2001; Mann *et al.* 2002a; Abbott *et al.* 2010). Some other studies suggest cooler temperatures in the new coastal settings due to marine transgression and extensive seasonal sea ice (Sancetta & Robinson 1983; Ager 2003). Our study demonstrates the onset of thermokarst lake development and therefore permafrost degradation as early as the Lateglacial with continued lake evolution and changes throughout the Holocene.

Carbon cycling

Thermokarst lake dynamics and maturation of the periglacial landscape at our study site had a direct influence on carbon availability and storage. The first lake generations expanding into yedoma can cause substantial methane emissions from freshly thawed late Pleistocene permafrost (Walter *et al.* 2006; Kessler *et al.* 2012). Such lakes may have contributed, in turn, to climate warming at the Pleistocene–Holocene transition (Walter *et al.* 2007). Grandma Rhonda lake developed under a Lateglacial climate and eroded into Pleistocene yedoma deposits, which at that time were most probably not yet covered with a significant organic layer or peat; hence, comparably little organic matter entered the lake as indicated by an average TOC content of only 2.7% in Unit B. The internal bioproductivity of the lake was dominated by algae (C/N of 10.4 in Unit B), possibly related to still rather cold climate conditions. Throughout the warmer Holocene submerged water plants were probably more abundant in Mama Rhonda lake and a thicker soil organic layer accumulated in the catchment of the developing thermokarst lake, resulting in an accelerated input of terrestrial organic matter into Mama Rhonda lake as a result of eroding shorelines (C/N of 14.6 and TOC of 8.6% in Unit C, excluding the tephra layers). Thus, TOC in Holocene Mama Rhonda lake sediments exceeds TOC in Lateglacial Grandma Rhonda lake sediments by a factor of 3 (or 3.2 when excluding tephra layers in Mama Rhonda lake sediments). In contrast, Walter Anthony *et al.* (2014) found in 40 drained refrozen thermokarst basins in Siberia, on average, a 1.6 times larger carbon accumulation in Holocene thermokarst lake sediments than in late Pleistocene deposits. Because the Grandma Rhonda lake sediments remained unfrozen below Mama Rhonda lake, decomposition and release of carbon over a long time period probably additionally reduced the carbon stock in Grandma Rhonda lake sediments.

Like most lake basins after drainage (Hinkel *et al.* 2003; Bockheim *et al.* 2004; Jones *et al.* 2012; Regmi *et al.* 2012), the waterlogged soils of Mama Rhonda basin most probably became vegetated within the first 5–10 years and began to accumulate peat after 20–100 years had elapsed (Jones *et al.* 2012). At the Kit-43 coring site, terrestrial peat accumulated at a rate of 0.46 cm 10 a^{-1} to a total thickness of 40 cm. The organic carbon content of 38% highlights the carbon storage capacity of drained basins. The area of modern Lake Rhonda is expanding with a mean rate of 0.53 m a^{-1} and a maximum erosion rates of up to 2.6 m a^{-1} at its northern shore (Jones *et al.* 2011), so Mama Rhonda lake sediments and post-drainage peat are continuously incorporated into the next thermokarst lake and geochemical cycle.

Conclusions

Our study confirms previous observations of permafrost degradation and thermokarst development in Central Beringia in the Lateglacial and early Holocene. For the first time, multiple lake and basin generations were documented in a permafrost core. The main conclusions of this study are:

- Thermokarst lake initiation with thaw subsidence of *in situ* Devil Mountain Maar tephra occurred in the Lateglacial at 11 800 cal. a BP.
- Intensive thermokarst processes in the Lateglacial and early Holocene enabled the development of a

rapidly expanding lake system. While sediments of this lake system (Grandma Rhonda lake phase) were preserved in the bottom of the Kit-43 core, a small remnant of this older lake basin is preserved at the southern margin of our study basin, including an ice-wedge cast with Grandma Rhonda lake sediments at Kit-7.

- An abrupt change in the depositional environment around 9000 cal. a BP as recorded in the Kit-43 core indicates a shift to a rather shallow and more dynamic lake system (Mama Rhonda lake phase), temporally coinciding with the Grandma Rhonda lake drainage event recorded in the Kit-75 exposure south of our study site. This drainage was, most probably, partial, resulting in wetland peat accumulation at Kit-75; our site was still occupied by a smaller remnant lake (Mama Rhonda lake) that subsequently started expanding again and was affected by multiple Holocene lake-level changes due to coalescence with neighbouring lakes.
- Drainage of Mama Rhonda lake and subsequent peat accumulation in the late Holocene started with the Medieval Warm Period at 1060 cal. a BP. The isotopic composition of intra-sedimentary ice preserved the palaeo-active layer and top-down aggradation of permafrost after drainage. Uniform isotopic composition shows missing secondary isotope fractionation processes below a depth of 154 cm, which may indicate an open freezing system i.e. as a result of the vicinity of an adjacent lake. Both palaeo- and modern active layers were filled by summer precipitation.

Overall, the Kit-43 sediment record preserves intensive environmental change in a periglacial lowland of Central Beringia that contains ice-rich permafrost. Newly forming thermokarst lakes in Late Pleistocene yedoma had profound impacts on biogeochemical cycling by thawing and mobilizing previously frozen organic carbon and nutrients into aquatic environments. This study also emphasizes that later generation lakes have a higher potential to accumulate and decompose organic matter from erosion of organic-rich Holocene deposits if they persist in the landscape over long time periods and that peat layers developing after drainage are an important carbon source for future thermokarst lakes.

Acknowledgements. – Fieldwork was supported by NSF (ARC-0732735), NASA (NNX08AJ37G) and the US National Park Service. Additional funding was provided by the German Federal Ministry of Education and Research (BMBF Grant No. 01DJ14003), the Western Alaska Landscape Conservation Cooperative Project (WA2011-02), RFBR (#16-040045-a) and the ERC (#338335). J. Lenz was supported by a Christiane Nüsslein-Volhard-Foundation grant, a dissertation stipend from the University of Potsdam, and the Helmholtz Graduate School for Polar and Marine Research (POLMAR), and acknowledges an invitation by S. Mischke to the Faculty of Earth Sciences (University of Iceland) for a research visit to finalize this study. We thank K. Walter Anthony and L. Farquharson for field support and discussions, and A. Myrbo and L. Farquharson for assisting with core splitting, imaging and GEOTEK scanning at the LacCore facility at the University of Minnesota. Further, we would like to thank H. Kemnitz, I. Schäpan, S. Wulf and O. Appelt (GFZ) for facilitating SEM imaging as well as geochemical analyses of tephra. We thank L. Farquharson, S. Lauterbach and one anonymous reviewer for providing helpful comments that improved the manuscript. Any use of trade, product or firm names is for descriptive purposes only and does not imply endorsement by the US Government.

References

Abbott, M. B., Edwards, M. E. & Finney, B. P. 2010: A 40,000-year record of environmental change from Burial Lake in northwest Alaska. *Quaternary Research 74*, 156–165.

Ager, T. 2003: Late Quaternary vegetation and climate history of the central Bering Land Bridge from St. Michael Island, western Alaska. *Quaternary Research 60*, 19–32.

Arp, C. D. & Jones, B. M. 2009: Geography of Alaska lake districts: Identification, description, and analysis of lake-rich regions of a diverse and dynamic state. *U.S. Geological Survey Scientific Investigations Report 2008-5215*, 40 pp.

Bartlein, P. J., Anderson, K. H., Anderson, P. M., Edwards, M. E., Mock, C. J., Thompson, R. S., Webb, R. S., Webb, T. III & Whitlock, C. 1998: Paleoclimatic simulations for North America over the past 21,000 years: features of the simulated climate and comparisons with paleoenvironmental data. *Quaternary Science Reviews 17*, 549–585.

Begét, J. E., Hopkins, D. M. & Charron, S. D. 1996: The largest known maars on Earth, Seward Peninsula, northwest Alaska. *Arctic 49*, 62–69.

Bigelow, N. H. & Edwards, M. E. 2001: A 14,000 yr paleoenvironmental record from Windmill Lake, Central Alaska: lateglacial and Holocene vegetation in the Alaska range. *Quaternary Science Reviews 20*, 203–215.

Billings, W. D. & Peterson, K. M. 1980: Vegetational change and ice-wedge polygons through the thaw-lake cycle in Arctic Alaska. *Arctic and Alpine Research 12*, 413–432.

Biskaborn, B. K., Herzschuh, U., Bolshiyanov, D. Y., Savelieva, L., Zibulski, R. & Diekmann, B. 2013a: Late Holocene thermokarst variability inferred from diatoms in a lake sediment record from the Lena Delta, Siberian Arctic. *Journal of Paleolimnology 49*, 155–170.

Biskaborn, B. K., Herzschuh, U., Bolshiyanov, D. Y., Schwamborn, G. & Diekmann, B. 2013b: Thermokarst processes and depositional events in a tundra lake, northeastern Siberia. *Permafrost and Periglacial Processes 24*, 160–174.

Blaauw, M. & Christen, J. A. 2011: Flexible palaeoclimate age-depth models using an Autoregressive Gamma Process. *Bayesian Analysis 6*, 457–474.

Bockheim, J. G., Hinkel, K. M., Eisner, W. R. & Dai, X. Y. 2004: Carbon pools and accumulation rates in an age-series of soils in drained thaw-lake basins, Arctic Alaska. *Soil Science Society of America Journal 68*, 697–704.

Brosius, L. S., Walter Anthony, K. M., Grosse, G., Chanton, J. P., Farquharson, L. M., Overduin, P. P. & Meyer, H. 2012: Using the deuterium isotope composition of permafrost meltwater to constrain thermokarst lake contributions to atmospheric CH_4 during the last deglaciation. *Journal of Geophysical Research 117*, G01022, doi: 10.1029/2011JG001810.

Cohen, A. S. 2003: *Paleolimnology: The History and Evolution of Lake Systems.* 528 pp. Oxford University Press, Oxford.

Colinvaux, P. A. 1964: The environment of the Bering Land Bridge. *Ecological Monographs 34*, 296–329.

Craig, H. 1961: Isotopic variations in meteoric waters. *Science 133*, 1702–1703.

Dansgaard, W. 1964: Stable isotopes in precipitation. *Tellus 16*, 436–468.

Detterman, R. L. 1970: Early Holocene warm interval in northern Alaska. *Arctic 23*, 130–132.

Edwards, M. E., Mock, C. J., Finney, B. P., Barber, V. & Bartlein, P. J. 2001: Potential analogues for paleoclimatic variations in eastern interior Alaska for the past 14,000 years: atmospheric-circulation controls of regional temperature and moisture responses. *Quaternary Science Reviews 20*, 189–202.

Edwards, M. E., Grosse, G., Jones, B. M. & McDowell, P. In press: The evolution of a thermokarst-lake landscape: late-Quaternary permafrost degradation and stabilization in interior Alaska. *Sedimentary Geology*, doi: 10.1016/j.sedgeo.2016.01.018.

Elias, S. A. 2000: Late Pleistocene climates of Beringia, based on analysis of fossil beetles. *Quaternary Research 53*, 229–235.

Elias, S. A. 2001: Beringian paleoecology: results from the 1997 workshop. *Quaternary Science Reviews 20*, 7–13.

Elias, S. A., Short, S. K. & Birks, H. H. 1997: Late Wisconsin environments of the Bering Land Bridge. *Palaeogeography, Palaeoclimatology, Palaeoecology 136*, 293–308.

van Everdingen, R. (ed.) 1998: *Multi-language Glossary of Permafrost and Related Ground-ice Terms.* National Snow and Ice Data Centre, Boulder.

Farquharson, L. M., Walter Anthony, K. M., Bigelow, N., Edwards, M. E. & Grosse, G. In press: Facies analysis of yedoma thermokarst lakes on the northern Seward Peninsula, Alaska. *Sedimentary Geology*, doi: 10.1016/j.sedgeo.2016.01.002.

French, H. & Shur, Y. 2010: The principles of cryostratigraphy. *Earth-Science Reviews 101*, 190–206.

French, H. M. & Millar, S. W. S. 2014: Permafrost at the time of the Last Glacial Maximum (LGM) in North America. *Boreas 43*, 667–677.

Fritz, M., Wolter, J., Rudaya, N., Palagushkina, O., Nazarova, L., Obu, J., Rethemeyer, J., Lantuit, H. & Wetterich, S. In press: Holocene ice-wedge polygon development in the northern Yukon, Canada. *Quaternary Science Reviews*, doi: 10.1016/j.quascirev.2016.02.008.

Gaglioti, B. V., Mann, D. H., Jones, B. M., Pohlman, J. W., Kunz, M. L. & Wooller, M. J. 2014: Radiocarbon age-offsets in an arctic lake reveal the long-term response of permafrost carbon to climate change. *Journal of Geophysical Research: Biogeosciences 119*, 1630–1651.

Goetcheus, V. G. & Birks, H. H. 2001: Full-glacial upland tundra vegetation preserved under tephra in the Beringia National Park, Seward Peninsula, Alaska. *Quaternary Science Reviews 20*, 135–147.

Grosse, G., Romanovsky, V. E., Jorgenson, T., Walter Anthony, K. M., Brown, J. & Overduin, P. P. 2011: Vulnerability and feedbacks of permafrost to climate change. *EOS 92*, 73–80.

Harry, S. A. & French, H. M. 1983: The orientation and evolution of thaw lakes, southwest Banks Island, Canadian Arctic. In Embleton, C. (ed.): *Proceedings of the 4th International Conference on Permafrost*, 456–461. National Academies Press, Washington, DC, USA.

Hinkel, K. M., Eisner, W. R., Bockheim, J. G., Nelson, F. E., Peterson, K. M. & Dia, X. Y. 2003: Spatial extent, age and carbon stocks of drained thaw lake basins on the Barrow Peninsula, Alaska. *Arctic, Antarctic, and Alpine Research 35*, 291–300.

Hinkel, K. M., Jones, B. M., Eisner, W. R., Cuomo, C. J., Beck, R. A. & Frohn, R. 2007: Methods to assess natural and anthropogenic thaw lake drainage on the western Arctic coastal plain of northern Alaska. *Journal of Geophysical Research 112*, F02S16 doi: 10.1029/2006JF000584.

Höfle, C., Edwards, M. E., Hopkins, D. M., Mann, D. H. & Ping, C. L. 2000: The full-glacial environment of the northern Seward Peninsula, Alaska, reconstructed from the 21,500 year old Kitluk paleosol. *Quaternary Research 53*, 143–153.

Hopkins, D. M. 1959: Cenozoic history of the Bering Land Bridge. *Science 129*, 1519–1528.

Hopkins, D. M. 1967. *The Bering Land Bridge*. 495 pp. Stanford University Press, Stanford.

Hopkins, D. M. 1988: The Espenberg Maars: a record of explosive volcanic activity in the Devil Mountain-Cape Espenberg area, Seward Peninsula, Alaska. *In* Schaaf, J. (ed.): *The Bering Land Bridge: An Archeological Survey*, 188–247. U.S. National Park Service, Nome.

Hopkins, D. M. & Kidd, J. G. 1988: Thaw lake sediments and sedimentary environments. *In* Senneset, K. (ed.): *5th International Permafrost Conference,* 790–795. Tapir Publishers, Trondheim.

Hopkins, D. M., Smith, P. A. & Matthews, J. V. Jr 1981: Dated wood from Alaska and the Yukon: implications for forest refugia in Beringia. *Quaternary Research 15*, 217–249.

Hugelius, G., Strauss, J., Zubrzycki, S., Harden, J. W., Schuur, E. A. G., Ping, C.-L., Schirrmeister, L., Grosse, G., Michaelson, G. J., Koven, C. D., O'Donnell, J. A., Elberling, B., Mishra, U., Camill, P., Yu, Z., Palmtag, J. & Kuhry, P. 2014: Estimated stocks of circumpolar permafrost carbon with quantified uncertainty ranges and identified data gaps. *Biogeosciences 11*, 6573–6593.

Hunt, J. B. & Hill, P. G. 1996: An inter-laboratory comparison of the electron probe microanalysis of glass geochemistry. *Quaternary International 34–36*, 229–241.

Hunt, S., Yu, Z. & Jones, M. E. 2013: Lateglacial and Holocene climate, disturbance and permafrost peatland dynamics on the Seward Peninsula, western Alaska. *Quaternary Science Reviews 63*, 42–58.

Jones, B. M. & Arp, C. D. 2015: Observing a catastrophic thermokarst lake drainage in northern Alaska. *Permafrost and Periglacial Processes 26*, 119–128.

Jones, M. C. & Yu, Z. 2010: Rapid deglacial and early Holocene expansion of peatlands in Alaska. *Proceedings of the National Academy of Sciences of the United States of America 107*, 7347–7352.

Jones, M. C., Grosse, G., Jones, B. M. & Walter Anthony, K. M. 2012: Peat accumulation in drained thermokarst lake basins in continuous, ice-rich permafrost, northern Seward Peninsula, Alaska. *Journal of Geophysical Research 117*, G00M07, doi: 10.1029/2011JG001766.

Jones, B. M., Grosse, G., Arp, C. D., Jones, M. C., Walter Anthony, K. M. & Romanovsky, V. E. 2011: Modern thermokarst lake dynamics in the continuous permafrost zone, northern Seward Peninsula, Alaska. *Journal of Geophysical Research 116*, G00M03, doi: 10.1029/2011JG001666.

Jorgenson, M. T. & Shur, Y. 2007: Evolution of lakes and basins in northern Alaska and discussion of the thaw lake cycle. *Journal of Geophysical Research 112*, F02S17, doi: 10.1029/2006JF000531.

Jorgenson, M. T., Yoshikawa, K., Kanevskiy, M., Shur, Y. L., Romanovsky, V. E., Marchenko, S., Grosse, G., Brown, J. & Jones, B. M. 2008: Permafrost characteristics of Alaska. In Kane, D. & Hinkel, K. (eds): *Proceedings of the 9th International Conference on Permafrost, 121–122*. University of Alaska, Fairbanks.

Kanevskiy, M., Shur, Y., Fortier, D., Jorgenson, M. T. & Stephani, E. 2011: Cryostratigraphy of late Pleistocene syngenetic permafrost (yedoma) in northern Alaska, Itkillik River exposure. *Quaternary Research 75*, 584–596.

Kaplina, T. N. & Lozhkin, A. V. 1980: Age of alass deposits of the Maritime Lowland of Yakutia. *International Geology Review 22*, 470–476.

Kaufman, D. S. & Hopkins, D. M. 1985: Late Cenozoic radiometric dates, Seward and Baldwin Peninsulas, and adjacent continental shelf, Alaska. *US Geological Survey, Open-File Report 85-374*, 28 pp.

Kaufman, D. S., Ager, T. A., Anderson, N. J., Anderson, P. M., Andrews, J. T., Bartlein, P. J., Brubaker, L. B., Coats, L. L., Cwynar, L. C., Duvall, M. L., Dyke, A. S., Edwards, M. E., Eisner, W. R., Gajewski, K., Geirsdóttir, A., Hu, F. S., Jennings, A. E., Kaplan, M. R., Kerwin, M. W., Lozhkin, A. V., MacDonald, G. M., Miller, G. H., Mock, C. J., Oswald, W. W., Otto-Bleisner, B. L., Porinchu, D. F., Rühland, K., Smol, J. P., Steig, E. J. & Wolfe, B. B. 2004: Holocene thermal maximum in the western Arctic (0–180° W). *Quaternary Science Reviews 23*, 529–560.

Kaufman, D. S., Anderson, R. S., Hu, F. S., Berg, E. & Werner, A. 2010: Evidence for a variable and wet Younger Dryas in Southern Alaska. *Quaternary Science Reviews 29*, 1445–1452.

Kaufman, D. S., Axford, Y. L., Henderson, A. C. G., McKay, N. P., Oswald, W. W., Saenger, C., Anderson, R. S., Bailey, H. L., Clegg, B., Gajewski, K., Hu, F. S., Jones, M. C., Massa, C., Routson, C. C., Werner, A., Wooller, M. J. & Yu, Z. C. In press: Holocene climate changes in eastern Beringia (NW North America) – A systematic review of multi-proxy evidence. *Quaternary Science Reviews*, doi: 10.1016/j.quascirev.2015.10.021.

Kessler, M. A., Plug, L. J. & Walter Anthony, K. M. 2012: Simulating the decadal- to millennial-scale dynamics of morphology and sequestered carbon mobilization of two thermokarst lakes in NW Alaska. *Journal of Geophysical Research 117*, G00M06 doi: 10.1029/2011JG001796.

Kokorowski, H., Anderson, P., Mock, C. & Lozhkin, A. 2008: A re-evaluation and spatial analysis of evidence for a Younger Dryas climatic reversal in Beringia. *Quaternary Science Reviews 27*, 1710–1722.

Kuehn, S. C., Froese, D. G., Shane, P. A. R. & Intercomparison Participants (INTAV) 2011: The INTAV intercomparison of electron-beam microanalysis of glass by tephrochronology laboratories: results and recommendations. *Quaternary International 246*, 19–47.

Kuzmina, S., Elias, S., Matheus, P., Storer, J. E. & Sher, A. 2008: Paleoenvironmental reconstruction of the Last Glacial Maximum, inferred from insect fossils from a tephra buried soil at Tempest Lake, Seward Peninsula, Alaska. *Palaeogeography, Palaeoclimatology, Palaeoecology 267*, 245–255.

Lamoureux, S. F. & Gilbert, R. 2004: Physical and chemical properties and proxies of high latitude lake sediments. *In* Pienitz, R., Douglas, M. S. V. & Smol, J. P. (eds.): *Long-term Environmental Change in Arctic and Antarctic Lakes 8*, 53–87. Springer, Dordrecht.

Lenz, J., Fritz, M., Schirrmeister, L., Lantuit, H., Wooller, M. J., Pollard, W. H. & Wetterich, S. 2013: Periglacial landscape dynamics in the western Canadian Arctic: results from a thermokarst lake record on a push moraine (Herschel Island, Yukon Territory). *Palaeogeography, Palaeoclimatology, Palaeoecology 381–382*, 15–25.

Lenz, J., Grosse, G., Jones, B. M., Walter Anthony, K. M., Bobrov, A., Wulf, S. & Wetterich, S. 2016: Mid-Wisconsin to Holocene permafrost and landscape dynamics based on a drained lake basin core from the northern Seward Peninsula, northwest Alaska. *Permafrost and Periglacial Processes 27*, 56–75.

MacDonald, L. A., Turner, K. W., Balasubramaniam, A. M., Wolfe, B. B., Hall, R. I. & Sweetman, J. N. 2012: Tracking hydrological responses of a thermokarst lake in the Old Crow Flats (Yukon Territory, Canada) to recent climate variability using aerial photographs and paleolimnological methods. *Hydrological Processes 26*, 117–129.

Mackay, J. R. 1997: A full-scale field experiment (1978–1995) on the growth of permafrost by means of lake drainage, western Arctic coast: a discussion of the method and some results. *Canadian Journal of Earth Sciences 34*, 17–33.

Mann, D. H., Groves, P., Reanier, R. E. & Kunz, M. L. 2010: Floodplains, permafrost, cottonwood trees, and peat: what happened the last time climate warmed suddenly in arctic Alaska? *Quaternary Science Reviews 29*, 3812–3830.

Mann, D. H., Heiser, P. A. & Finney, B. P. 2002b: Holocene history of the Great Kobuk Sand Dunes, northwestern Alaska. *Quaternary Science Reviews 21*, 709–731.

Mann, D. H., Peteet, D. M., Reanier, R. E. & Kunz, M. L. 2002a: Responses of an arctic landscape to late glacial and early Holocene climatic changes: the importance of moisture. *Quaternary Science Reviews 21*, 997–1021.

Matthews, J. V. Jr 1974: Quaternary environments at Cape Deceit (Seward Peninsula, Alaska): evolution of a tundra ecosystem. *Geological Society of America Bulletin 85*, 1353–1384.

McCulloch, D. & Hopkins, D. 1966: Evidence for an early recent warm interval in Northwestern Alaska. *Geological Society of America Bulletin 77*, 1089–1108.

Meyer, H., Schirrmeister, L., Yoshikawa, K., Opel, T., Wetterich, S., Hubberten, H.-W. & Brown, J. 2010: Permafrost evidence for severe winter cooling during the Younger Dryas in northern Alaska. *Geophysical Research Letters 37*, L03501, doi: 10.1029/2009GL041013.

Meyer, H., Schönicke, L., Wand, U., Hubberten, H.-W. & Friedrichsen, H. 2000: Isotope studies of hydrogen and oxygen in ground ice – experiences with the equilibration technique. *Isotopes in Environmental and Health Studies 36*, 133–149.

Meyers, P. A. 1997: Organic geochemical proxies of paleoceanographic, paleolimnologic, and paleoclimatic processes. *Organic Geochemistry 27*, 213–250.

Meyers, P. A. & Takemura, K. 1997: Quaternary changes in delivery and accumulation of organic matter in sediments in Lake Biwa, Japan. *Journal of Paleolimnology 18*, 211–218.

Michel, F. A., Fritz, P. & Drimmie, R. I. 1989: Evidence of climatic change from oxygen and carbon isotope variations in sediments of a small arctic lake. *Canadian Journal of Quaternary Science 4*, 201–209.

Morgenstern, A., Ulrich, M., Günther, F., Roessler, S., Fedorova, I., Rudaya, N., Wetterich, S., Boike, J. & Schirrmeister, L. 2013: Evolution of thermokarst in East Siberian ice-rich permafrost: a case study. *Geomorphology 201*, 363–379.

Munsell Color Company 1994: *Munsell Soil Color Charts.* Macbeth Division of Kollmorgen Instruments Corporation, New Windsor, NY.

Nelson, R. E. & Carter, L. D. 1987: Paleoenvironmental analysis of insects and extralimital *Populus* from an Early Holocene site on the Arctic Slope of Alaska. *Arctic and Alpine Research 19*, 230–241.

Nowacki, G. J., Spencer, P., Fleming, M. & Jorgenson, T. 2002: Unified ecoregions of Alaska, *US. Geological Survey, Open File Report 02-297*.

Olthof, I., Robert, H. F. & Schmitt, C. 2015: Landsat-based mapping of thermokarst lake dynamics on the Tuktoyaktuk Coastal Plain, Northwest Territories, Canada since 1985. *Remote Sensing of Environment 168*, 194–204.

Oswald, W. W., Brubaker, L. B. & Anderson, P. M. 1999: Late Quaternary history of the Howard Pass area, northwestern Alaska. *Canadian Journal of Botany 77*, 570–581.

Peltier, W. R. & Fairbanks, R. G. 2006: Global glacial ice volume and Last Glacial Maximum duration from an extended Barbados sea level record. *Quaternary Science Reviews 25*, 3322–3337.

Rampton, V. M. 1988: Quaternary geology of the Tuktoyaktuk coastlands, Northwest Territories. *Geological Survey of Canada, Memoir 423*, 98 pp.

Regmi, P., Grosse, G., Jones, M. J., Jones, B. M. & Walter Anthony, K. M. 2012: Characterizing post-drainage succession in thermokarst lake basins on the Seward Peninsula, Alaska with TerraSAR-X backscatter and Landsat-based NDVI data. *Remote Sensing 4*, 3741–3765.

Reimer, P., Bard, E., Bayliss, A., Beck, J., Blackwell, P., Bronk Ramsey, C., Buck, C., Cheng, H., Edwards, R., Friedrich, M., Grootes, P., Guilderson, T., Haflidason, H., Hajdas, I., Hatté, C., Heaton, T., Hoffmann, D., Hogg, A., Hughen, K., Kaiser, K., Kromer, B., Manning, S., Niu, M., Reimer, R., Richards, D., Scott, E., Southon, J., Staff, R., Turney, C. & van der Plicht, J. 2013: IntCal13 and Marine13 radiocarbon age calibration curves 0–50,000 years cal BP. *Radiocarbon 55*, 1869–1887.

Romanovsky, V. E., Sharon, L. S. & Christiansen, H. H. 2010: Permafrost thermal state in the polar Northern Hemisphere during the International Polar Year 2007–2009: a synthesis. *Permafrost and Periglacial Processes 21*, 106–116.

Sancetta, C. & Robinson, S. W. 1983: Diatom evidence on Wisconsin and Holocene events in the Bering Sea. *Quaternary Research 20*, 232–245.

Schleusner, P., Biskaborn, B. K., Kienast, F., Wolter, J., Subetto, D. & Diekmann, B. 2015: Basin evolution and palaeoenvironmental variability of the thermokarst lake El'gene-Kyuele, Arctic Siberia. *Boreas 44*, 216–229.

Schwamborn, G., Meyer, H., Schirrmeister, L. & Federov, A. 2014: Past freeze and thaw cycling in the margin of the El'gygytgyn crater deduced from a 141 m long permafrost record. *Climate of the Past 10*, 1109–1123.

Séjourné, A., Costard, F., Federov, A., Gargani, J., Skorve, J., Massé, A. & Mège, D. 2015: Evolution of the banks of thermokarst lakes in Central Yakutia (Central Siberia) due to retrogressive thaw slump activity controlled by insolation. *Geomorphology 241*, 31–40.

Smith, S. L., Romanovsky, V. E., Lewkowicz, A. G., Burn, C. R., Allard, M., Clow, G. D., Yoshikawa, K. & Throop, J. 2010: Thermal state of permafrost in North America: a contribution to the

International Polar Year. *Permafrost and Periglacial Processes 21*, 117–135.

Thompson, R., Battarbee, R. W., O'Sullivan, P. E. & Oldfield, F. 1975: Magnetic susceptibility of lake sediments. *Limnology and Oceanography 20*, 688–698.

Vandenberghe, J., French, H. M., Gorbunov, A., Marchenko, S., Velichko, A. A., Jin, H., Cui, Z., Zhang, T. & Wan, X. 2014: The Last Permafrost Maximum (LPM) map of the Northern Hemisphere: Permafrost extent and mean annual air temperatures, 25–17 ka BP. *Boreas 43*, 652–666.

Walter, K. M., Edwards, M. E., Grosse, G., Zimov, S. A. & Chapin, F. S. III 2007: Thermokarst lakes as a source of atmospheric CH_4 during the last deglaciation. *Science 318*, 633–636.

Walter, K. M., Zimov, S. A., Chanton, J. P., Verbyla, D. & Chapin, F. S. III 2006: Methane bubbling from Siberian thaw lakes as a positive feedback to climate warming. *Nature 443*, 71–75.

Walter Anthony, K. M., Zimov, S. A., Grosse, G., Jones, M. C., Anthony, P. M., Chapin, F. S. III, Finlay, J. C., Mack, M. C., Davydov, S., Frenzel, P. & Frolking, S. 2014: A shift of thermokarst lakes from carbon sources to sinks during the Holocene epoch. *Nature 511*, 452–456.

Washburn, A. L. 1980: Permafrost features as evidence of climatic change. *Earth-Science Reviews 15*, 327–402.

West, J. J. & Plug, L. J. 2008: Time-dependent morphology of thaw lakes and taliks in deep and shallow ground ice. *Journal of Geophysical Research Letters 113*, F01009, doi: 10.1029/2006JF000696.

Wetterich, S., Grosse, G., Schirrmeister, L., Andreev, A. A., Bobrov, A. A., Kienast, F., Bigelow, N. H. & Edwards, M. E. 2012: Late Quaternary environmental and landscape dynamics revealed by a pingo sequence on the northern Seward Peninsula, Alaska. *Quaternary Science Reviews 39*, 26–44.

Zona, D., Oechel, W. C., Peterson, K. M., Clements, R. J., Paw, U. K. T. & Ustin, S. L. 2010: Characterization of the carbon fluxes of a vegetated drained lake basin chronosequence on the Alaskan Arctic Coastal Plain. *Global Change Biology 16*, 1870–1882.

Supporting Information

Additional Supporting Information may be found in the online version of this article at http://www.boreas.dk and primary data is available on PANGAEA (doi: 10.1594/PANGAEA.859554).

Table S1. Lithological and geochemical measurements on core Kit-43 sediment and water samples, and measurements of magnetic susceptibility of the core in on average 1-cm increments.

Table S2. Single non-normalized data of electron probe analyses of all glass shard samples from the Seward Peninsula and the Lipari obsidian reference standard.